Benthic oxygen consumption rates during hypoxic conditions on the Oregon continental shelf: Evaluation of the eddy correlation method

Clare E. Reimers,[1] H. Tuba Özkan-Haller,[1] Peter Berg,[2] Allan Devol,[3] Kristina McCann-Grosvenor,[1] and Rhea D. Sanders[1]

Received 1 September 2011; revised 6 December 2011; accepted 11 December 2011; published 10 February 2012.

[1] Three stations, at ~80 m water depth on the Oregon shelf between 44.7°N and 43.9 N, were studied under hypoxic conditions in late spring and summer of 2009 to determine benthic oxygen consumption rates. Oxygen fluxes were derived from eddy correlation (EC) measurements made from an autonomous lander deployed for 11–15 h at a time. Average oxygen consumption rates ranged from 3.2 to 9.8 mmol m^{-2} d^{-1} and were highest at the southernmost station. Methods for separating eddy components and rotating coordinates were examined for effects on EC fluxes. It was found that oscillations at frequencies associated with surface and internal waves made significant contributions, but horizontal component biasing could be minimized by wave-based rotation methods. Additional measurements included benthic boundary layer properties, and sediment permeability and profiles of sediment organic C, chlorophyll-*a*, excess ^{210}Pb and % fines. Comparative flux estimates were determined from benthic chamber measurements and microelectrode profiles at two of the stations. The chamber O_2 consumption rates exceeded the EC fluxes by factors of 1.2–1.8, which may reflect enclosure effects, the different spatial and temporal scales of the measurements, and/or inhomogeneous benthic respiration rates. The magnitudes of the fluxes by either method, however, are low for shelf depths. Thus, for benthic O_2 consumption to contribute to Oregon shelf hypoxia, bottom waters must be slowly renewed and minimally ventilated by along- or across-shelf advection and turbulent mixing. Circulation studies indicate these conditions are favored by increased near-bottom stratification during persistent summer upwelling- relaxation cycles.

Citation: Reimers, C. E., H. T. Özkan-Haller, P. Berg, A. Devol, K. McCann-Grosvenor, and R. D. Sanders (2012), Benthic oxygen consumption rates during hypoxic conditions on the Oregon continental shelf: Evaluation of the eddy correlation method, *J. Geophys. Res.*, *117*, C02021, doi:10.1029/2011JC007564.

1. Introduction

[2] In recent years eddy correlation (EC) has gained acceptance as a valid technique for determining dissolved oxygen (O_2) fluxes between aquatic sediments and overlying water masses. To derive an O_2 eddy flux, the covariance between high-resolution fluctuations of both O_2 and vertical velocity measured above the sediment surface (typically at a height between 10 and 20 cm) is computed. Among EC's described advantages are that (1) measurements are made under natural light and hydrodynamic conditions, (2) the sediments are not enclosed or disturbed, and (3) derived fluxes reflect benthic O_2 exchange processes occurring over large sediment surface areas (tens of square meters) [*Berg et al.*, 2007]. EC aquatic applications are increasing and include studies of O_2 dynamics in a shallow river bed, two lakes, a variety of nearshore marine environments, and a deep marine bay [*Berg et al.*, 2003, 2009; *Kuwae et al.*, 2006; *McGinnis et al.*, 2008; *Brand et al.*, 2008; *Berg and Huettel*, 2008; *Glud et al.*, 2010; *Hume et al.*, 2011]. The method is analogous to the measurement of near-bottom, turbulence-induced heat and momentum fluxes often undertaken by physical oceanographers [e.g., *Shaw and Trowbridge*, 2001]. However, it also requires many of the same assumptions about conditions, mass balance, and data filtering-correction techniques that are used by boundary layer meteorologists to discriminate between good and erroneous gas flux measurements at land-atmosphere interfaces [e.g., *Finnigan*, 1999; *Finnigan et al.*, 2003; *Aubinet*, 2008]. Thus, these assumptions should be reevaluated in every new field situation.

[3] In this paper, EC measurements are reported that were made on the central Oregon continental shelf in late spring and summer of 2009 during conditions of coastal upwelling, hypoxia, and moderate wave energy. The acquisition of EC data in this dynamic and challenging environment was

[1]College of Oceanic and Atmospheric Sciences, Oregon State University, Corvallis, Oregon, USA.
[2]Department of Environmental Sciences, University of Virginia, Charlottesville, Virginia, USA.
[3]School of Oceanography, University of Washington, Seattle, Washington, USA.

0148-0227/12/2011JC007564

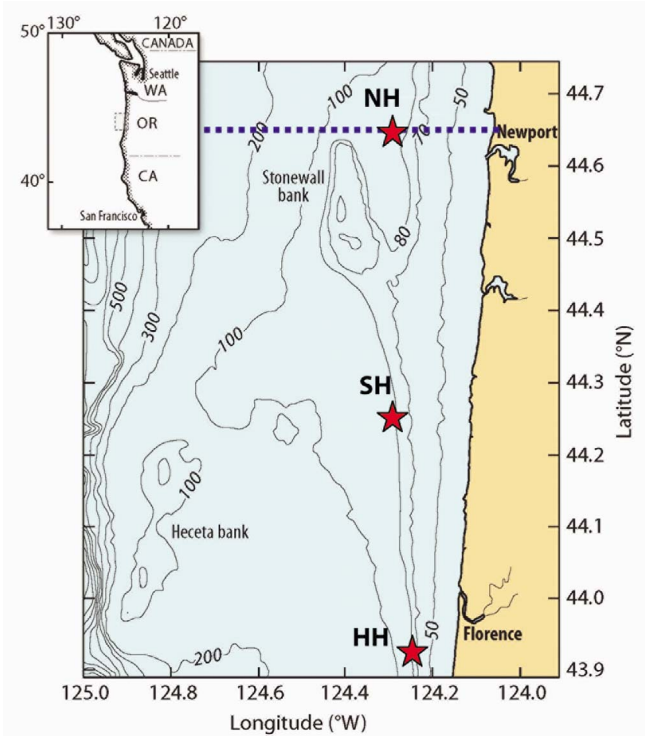

Figure 1. Bathymetric map of the central Oregon continental shelf showing the locations of the Newport hydrographic line (dotted line) and the study sites.

enabled by the development of a unique benthic tripod deployed in a moored mode and equipped with sensors and a rotating digital still camera. Simultaneous pressure data are used to evaluate the influences of the wave-induced velocity field on EC components. Detrending and coordinate rotation approaches are compared to adopt "best practices" for deriving O_2 eddy fluxes at these study sites and understanding what they represent in terms of a desired measure of the total benthic O_2 consumption rate.

[4] The central continental shelf of Oregon is part of a narrow oceanic eastern boundary current margin [*Chen et al.*, 2004; *Jahnke*, 2010] where equatorward winds intermittently drive offshore surface Ekman transport and the upwelling of cold, nutrient-rich and O_2-depleted water during spring and summer [*Barth et al.*, 2007; *Chan et al.*, 2008]; in contrast, large wind waves associated with North Pacific storm patterns dominate water column mixing during winter [*Allan and Komar*, 2006]. Spatial and temporal changes in phytoplankton production, the alongshore coastal jet, and a particle-enriched benthic boundary layer are expected to have an impact on patterns of organic matter transport and consequently respiration in both the water column and sediments [*Castelao and Barth*, 2005; *Perlin et al.*, 2005; *Hales et al.*, 2006]. Inshore of the 100 m isobath, the sediments are predominantly fine sand that is subject to resuspension and particulate organic matter entrapment (filtering) by both physical transport (including oscillatory ripple migration) and bioturbation [*Komar et al.*, 1972; *Kulm*, 1978]. These properties and processes, together with a potential for wave pumping of bottom water into the bed, complicate assessments of the benthic role in O_2 or coupled carbon budgets [*Riedl et al.*, 1972; *Shum and Sundby*, 1996; *Huettel and Webster*, 2001]. In fact, no measurements of benthic O_2 uptake made by traditional benthic chamber or microprofiling methods have been reported for sites <100 m on the Oregon shelf. *Devol and Christensen* [1993] do report chamber fluxes of -5 to -18 mmol O_2 m^{-2} d^{-1} from the neighboring Washington shelf, with the highest rates occurring at 114 m water depth associated with a midshelf silt deposit. Similarly, historic deficits of O_2 and nitrate that increase along salinity surfaces led *Connolly et al.* [2010] to infer that Washington shelf sediments are a regular sink for $\sim 1 \pm 0.2$ μM O_2 d^{-1} from the bottom boundary layer. This depletion rate suggests sediment respiration contributes to episodes of severe shelf hypoxia nearly equally with water column respiration [*Connolly et al.*, 2010].

[5] Certainly, an understanding of how ecosystem processes respond to local forcing or are linked to ocean basin-scale changes requires trusted baseline measurements. The EC technique produces rich data sets that yield information on local waves, currents, turbulence, and their impacts on benthic O_2 fluxes. In this paper we examine EC data from the Oregon shelf with a focus on three midshelf stations. Water column, sediment, O_2 microprofile, and benthic chamber data are also used to assess the along-shelf variability of organic carbon respiration and the comparability of EC oxygen fluxes with estimates from traditional methods.

2. Materials and Methods

2.1. Study Sites

[6] The study sites were occupied during cruises of the R/V *Wecoma* in June and August 2009. The stations are designated NH, SH, and HH for their proximity to the Newport (Oregon) hydrographic line and coastal features known as Strawberry Hill and Hecata Head, respectively [*Grantham et al.*, 2004]. They were located near the 80 m isobath in low-relief areas of sandy sediments at approximately 44.65°N, 124.30°W; 44.24°N, 124.32°W; and 43.93°N, 124.25°W, respectively (Figure 1).

2.2. BOXER: A Lander for Measuring Benthic Oxygen Exchange Rates by Eddy Correlation Together With Complementary Benthic Boundary Layer Information

[7] The autonomous benthic lander system for eddy correlation measurements, developed at Oregon State University, is specifically tailored for the dynamic shelf environments of the NE Pacific and deployments from regional or intermediate-scale research vessels. This Benthic Oxygen Exchange Rate (BOXER) lander (Figure 2) has the following principal components: (1) a sturdy, lead-weighted, wide-based frame (height 1.8 m, width 2.3 m) as a stable support platform for the instrumentation even under energetic waves and currents; (2) an acoustic velocimeter (6 MHz, Nortek Vector, with a fixed 3-D probe) for fast (up to 64 Hz) 3-D velocity measurements at a fixed position 10–20 cm above the seafloor; (3) a high-resolution autozeroing amplifier (developed at the Max Planck Institute for Marine Microbiology and produced by Unisense A/S) that couples to a microelectrode for fast low-noise O_2 measurements without flow sensitivity; (4) a time-lapse digital still camera and

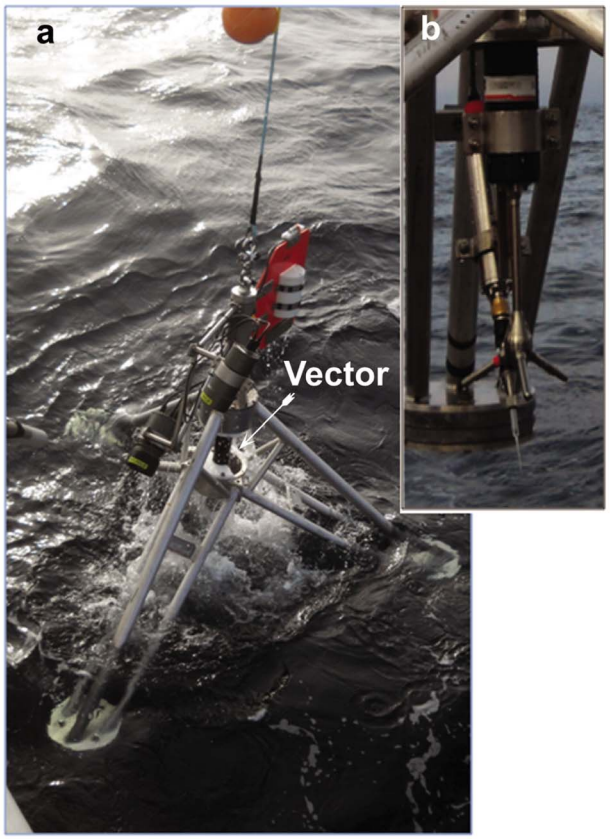

Figure 2. (a) Photo of the BOXER lander during deployment, and (b) an enlarged view of the Vector probe positioned with the O_2 microelectrode and amplifier.

strobe (Insite Pacific, Scorpio) with a counterbalancing vane on a rotating bearing assembly for observing the seafloor areas contributing to the flux; and (5) a light level and temperature-depth sensor (Wildlife Computers, MK-9) for independent near-bottom measurements (mounted on top of the camera vane).

[8] A newer EC measurement system (used for one of three deployments) also incorporates (6) a controller unit (developed by Unisense A/S) for deployment programming, power (12V, 18 h capacity by way of a rechargeable Li-ion battery pack), sensor synchronizing, calibration, and data logging (256 MB), and (7) an Aanderaa O_2 optode (model 4175) for independent O_2 monitoring.

[9] Prior to the introduction of the Unisense controller unit, the Nortek Vector was used to log all data as originally configured by *Berg et al.* [2009].

[10] BOXER was deployed by lowering with Spectra synthetic fiber line (5/8″) unwrapped from a winch drum and by releasing spar and surface buoys with an ~2:1 ratio of line length to water depth. Recovery occurred by picking up the buoys and using the winch to haul in the line and lander. The EC instrumentation was programmed to collect data at 64 Hz in 15 min bursts with 5 min between bursts. Initial and final bursts (i.e., those that included measurements <15 min before or after BOXER touched down or left the bottom) were excluded from reported data sets.

[11] The O_2 microelectrode readings were stored by time (t) as counts (cts), which were converted to O_2 concentrations according to

$$O_{2t} = (\mathrm{cts}_t - \mathrm{cts}_0) * O_{2\mathrm{BW}}/(\mathrm{cts}_{\mathrm{BW}} - \mathrm{cts}_0), \quad (1)$$

where cts_0 represents an average of predeployment readings of the mounted sensor when dipped in a chilled (~10°C) anoxic 10% solution of 1 M Na ascorbate and 0.5 M NaOH [*Andersen et al.*, 2001] (i.e., the zero calibration), and $\mathrm{cts}_{\mathrm{BW}}$ equals an average set of counts recorded simultaneously with an independent measurement of the bottom water O_2 concentration ($O_{2\mathrm{BW}}$). In this study all $O_{2\mathrm{BW}}$ values were assessed by Winkler titrations of triplicate water samples collected within 4 m of the bottom using a conductivity-temperature-depth (CTD) probe rosette (Seabird SBE 911 Plus), and $\mathrm{cts}_{\mathrm{BW}}$ values were calculated from the average readings during the 15 min burst coinciding with the time of bottom water sampling.

[12] It is a unique capability of the autozeroing amplifier to measure the constant (or DC) component of the O_2 signal over a preset period at the beginning of each burst, typically 30 s, and then for subsequent readings to subtract this signal from the total and amplify the difference 10 times, creating a fluctuating (or AC) signal. Both the total and amplified AC signals are recorded as counts. We derived O_{2t} using the more sensitive AC records. All O_2 and velocity time series were filtered of outliers (representing usually <1% of all measurements) using a phase-space method adapted from *Goring and Nikora* [2002] and replaced with points based on a spline fit to adjacent data. These "cleaned" velocity and O_2 time series were then reduced from 64 to 16 Hz by computing sequential four-point averages to filter out high-frequency noise.

[13] Another parameter measured by the Vector ADV is near-bottom pressure. Pressure time series were used to extract surface wave characteristics based on finite-depth linear water wave theory [*Dean and Dalrymple*, 1992]. Computations were carried out in the frequency domain after applying a low-pass filter to the pressure spectrum with a cutoff frequency that corresponds to the shortest wave that can still be observed by the pressure sensor (defined by linear water wave theory as $h/L = 1/2$, where h is the depth of the sensor and L is the wavelength associated with a wave at the cutoff frequency). All computations described in this and following sections were executed using MatLab (Mathworks®).

2.3. EC Oxygen Flux Analysis Techniques

[14] The benthic EC oxygen flux method pioneered by *Berg et al.* [2003, 2009] relies on assumptions of oxygen conservation in a control volume bounded below by the seafloor and above by the intersection of the measurement point (z_m) with an x-y coordinate plane that is parallel with the seafloor [*Hume et al.*, 2011]. The three-dimensional tracer conservation equation for this volume and the simplifying assumptions used in the EC technique to derive a representation of the seafloor O_2 source or sink are described by *Lorrai et al.* [2010], but can also be formulated from theoretical considerations given in papers such as those by *Finnigan* [1999] and *Feigenwinter et al.* [2004].

[15] To evaluate EC data sets, we first remove segments of clearly anomalous data. These segments may be over a few minutes up to an entire burst. Targeted anomalies are intervals with unusually large vertical velocities or what appear as isolated sharp dips in O_2 followed by a slower return to baseline O_2 readings. The depression in the O_2 signal may be explained by marine snow or other suspended material temporarily adhering to the microelectrode tip. The third type of anomaly arises when O_2 shifts abruptly from having a level mean to an increasing or decreasing trend, or vice versa, within a burst. Such shifts suggest short periods of microelectrode instability or a changing bottom water O_2 profile.

[16] A following step in the EC analysis is separating the velocity vectors and concentration measurements into time-average and fluctuating components (Reynolds decomposition) [*Lee et al.*, 2004; *Lorrai et al.*, 2010]. Herein, we define the time-average component to correspond to the mean over the entire deployment and further separate the fluctuating component into a low-frequency variation and higher-frequency variability (which are presumably due to waves and turbulence). Hence, the total time series for O_2 concentration, for example, is then expressed as $c(t) = \overline{c} + c_{\mathrm{lf}}(t) + c'(t)$. Velocity components are decomposed in a similar fashion with the conventional notation of an overbar to denote the time average and a prime to denote high-frequency fluctuating components. The low-frequency component is influenced by the length and separation of individual data bursts and identified using a detrending method, and the high-frequency fluctuating component can then be obtained by subtracting the identified mean and low-frequency components from the total signal. Three detrending methods are used to define the low-frequency fluctuating component and are compared below. These are (1) linear detrending (LD), (2) a centered running average (RA) (see definitions given by *Sakai et al.* [2001] and *Lee et al.* [2004]), or (3) a low-pass frequency filter (FF) [see *Bendat and Piersol*, 1971, chapter 9]. The latter (FF) filter has some similarities to the RA method, but it has the advantage of allowing for a precise understanding of the frequency content of the motions that are considered as part of the high-frequency components, and it does not have computational edge effects at the beginning and ends of bursts [*Bendat and Piersol*, 1971]. We note here that, by definition, the average values (over the whole deployment) of the fluctuating components are zero; hence $\overline{c_{\mathrm{lf}}} = \overline{c'} = 0$ holds. Further, the average over individual bursts of the high-frequency fluctuating component also vanishes by definition.

[17] The resulting net vertical flux (averaged over the entire deployment) is

$$\overline{\mathrm{flux}} = \overline{wc} = \overline{w}\,\overline{c} + \overline{w_{\mathrm{lf}} c_{\mathrm{lf}}} + \overline{w'c'}. \qquad (2)$$

When $\overline{w} \neq 0$, it is generally assumed that vertical advection $(\overline{w}\,\overline{c})$ does not represent a component of the seafloor exchange rate because this transport is balanced simultaneously by transient horizontal advection events [*Finnigan et al.*, 2003]. Unfortunately, this balance cannot be constrained from the information available from a single point in the benthic boundary layer. The practice of coordinate rotation so that the mean velocity defines the x axis (and therefore the rotated velocities are such that $\overline{v_R} = \overline{w_R} = 0$) is used instead by some authors to mathematically force vertical advection terms to zero. This can be appropriate if horizontal flow is strong and consistently at an angle relative to the seabed. The complication is with complex flow or short averaging periods (relative to the periods of all contributing eddies); these rotations may unpredictably fold horizontal components into the eddy flux. Furthermore, rotation procedures may be applied so that $\overline{v_R} = \overline{w_R} = 0$ for each sampling burst, creating multiple coordinate systems, or applied once with reference to the full data record. We examine possible biases generated or removed by different rotation methods as part of the results.

[18] The low-frequency flux $(\overline{w_{\mathrm{lf}} c_{\mathrm{lf}}})$ is generally nonzero and, in our case, is defined to result from variability at the scales of hours to days. For example, tidal variability or changes in the ocean properties due to upwelling fronts will contribute to this flux. It is assumed that a sufficiently long deployment period would capture multiple cycles of these low-frequency motions and would therefore lead to a low-frequency flux that averages to zero in the long term. We note that the deployments that will be discussed herein are not of such durations, and nonzero low-frequency fluxes are observed.

[19] Finally, the flux $\overline{(w'c')}$ in equation (2) represents all dynamic processes that contribute a net nonzero flux of oxygen into the seabed where it is consumed. Turbulence in the water column undoubtedly contributes greatly to this net flux, but recent work [*Huettel and Webster*, 2001; *Precht et al.*, 2004] has suggested that processes related to surface wave motions or flow-induced pressure gradients around small-scale sediment topography may also contribute. For example, wave orbital velocities near a rippled sandy bed may lead to significant flow velocities through the bed, allowing higher rates of oxygen consumption to occur and water of lower O_2 concentration to be returned to the water column [*Reimers et al.*, 2004].

[20] However, net flux computations across wave frequencies can be significantly biased if the observation platform is not oriented perfectly in the vertical direction. Any rotation errors will result in components of the large horizontal velocities associated with surface waves being mapped onto the vertical velocities [*Shaw and Trowbridge*, 2001]. Methods for removing the wave flux components have been under development [e.g., *Shaw and Trowbridge*, 2001], but cannot be applied here because they require the presence of multiple velocity sensors. Further, these methods remove the entire wave contribution, not distinguishing between the real wave contribution and the apparent wave bias due to rotation errors.

[21] Given our interest in the net vertical flux and the possibility for an actual wave contribution, we instead consider utilizing information about the waves from the Vector's colocated pressure sensor to adjust the orientation of the observations. In particular, the criteria established were first to rotate in the horizontal so the horizontal wave signal is primarily contained in the u velocities. Hence, the x axis is aligned with the general propagation direction of the waves. Next, a vertical rotation is established, minimizing the difference between the observed vertical velocity (at the wave frequencies) and the vertical velocity derived via linear water wave theory from the pressure signal. For our data sets, this amounts to a minimization of the wave signal in the vertical velocity component.

Table 1. Characteristics of Bottom Water Samples[a]

Station	Date and Local Time (hhmm)	Height Above Bottom (m)	Oxygen[b] (μM)	POC (μM)	PN (μM)	OC:N$_a$	Nitrate and Nitrite (μM)	Phosphate (μM)	Silicate (μM)	Ammonia (μM)	Salinity	Temperature (°C)	Sigma-Theta (kg/m^3)
NH	7 Jun 2009, 2108	2.4	59.0 ± 0.2	9.45 ± 0.25	1.28 ± 0.10	7.4	34.4 ± 0.1	2.78 ± 0.00	63.8 ± 0.0	0.01 ± 0.01	33.92	7.03	26.57
NH[c]	8 Jun 2009, 2029	2.4	60.3 ± 0.6	ND[d]	ND	ND	34.9 ± 0.4	2.80 ± 0.01	62.6 ± 0.3	0.02 ± 0.01	33.92	7.04	26.56
NH	20 Aug 2009, 2045	2.3	44.8 ± 0.3	4.58 ± 0.32	0.67 ± 0.07	6.8	34.8 ± 0.0	3.01 ± 0.03	62.8 ± 0.9	0.00 ± 0.01	33.84	7.57	26.43
SH	13Jun 2009, 1808	3.8	40.8 ± 0.2	55.36 ± 9.55	7.75 ± 0.93	7.1	32.7 ± 0.0	3.15 ± 0.06	68.2 ± 0.2	0.91 ±0.11	33.84	7.36	26.45
SH[c]	18 Aug 2009, 2012	2.6	62.0 ± 0.3	10.94 ± 1.76	1.41 ± 0.23	7.8	32.4 ± 0.0	3.01 ± 0.00	63.9 ± 0.1	1.85 ± 0.02	33.86	7.71	26.43
SH	21 Aug 2009, 1953	1.3	62.1 ± 1.8	6.80 ± 0.38	0.96 ± 0.10	7.1	31.5 ± 0.1	2.96 ± 0.01	63.1 ± 0.5	2.23 ± 0.03	33.84	7.78	26.40
HH[c]	11 Jun 2009, 1806	2.7	52.8 ± 0.1	16.58 ± 0.60	2.07 ± 0.07	8.0	33.7 ± 0.0	3.06 ± 0.05	61.5 ± 0.2	1.24 ± 0.35	33.84	7.41	26.45

[a]All discrete analyses are from three individual Niskin bottles. Times based on first bottle mark. Uncertainties represent ±1 SD.
[b]Based on Winkler titration.
[c]Cast coinciding with BOXER deployment.
[d]ND, not determined.

[22] The resulting flux term ($\overline{w'c'}$) is herein referred to as the EC oxygen flux or eddy flux. This net flux will contain contributions from turbulence as well as from wave-induced processes. These are discussed in detail as part of the results. To facilitate some understanding of the contribution of the two processes, the EC flux can also be expressed as

$$\overline{w'c'} = \int_0^{f_{\max}} \mathrm{Co}_{w'c'}(f)df, \tag{3}$$

where $\mathrm{Co}_{w'c'}$ is the cospectrum of $w'c'$, f is the frequency, and $f_{\max}$ is the upper frequency limit constrained by the sampling frequency [*Berg et al.*, 2003; *Lorrai et al.*, 2010]. The sign convention is that vertical fluxes out of the base of the control volume and into the seabed are negative. Generally, in this study we average a series of eddy flux estimates from data records of 14 or 14.5 min (individual 15 min bursts minus the autozeroing amplifier adjust time), resulting in a frequency resolution of either 0.0012 or 0.0011 Hz. Cospectra are calculated for each burst using the Fourier transform of the fluctuating components w' and c' utilizing a simple Dirichlet window. The cospectrum is then computed as the product of the transformed w' and the conjugate of the transformed c' with no further band averaging.

2.4. Complementary Bottom Water and Sediment Measurements

[23] As noted previously, we routinely conducted a CTD-rosette cast during each BOXER deployment. The CTD package was equipped with additional sensors, including probes for O_2 (SBE 43) and transmissometry (Chelsea/Seatech/Wetlab CStar). The CTD was lowered to within 4 m of the seafloor and three 10 L Niskin bottles tripped in a rapid sequence (Table 1). Generally, each of these bottles was subsampled aboard ship for O_2, nutrients, and particulate organic C and N (POC/PN) concentrations. The CTD sensor data were processed using the Sea-Bird SEASOFT software and laboratory calibration files to obtain 1 dbar average values of pressure, temperature, conductivity, salinity, density, dissolved O_2 concentration, and beam transmission. Oxygen concentrations were measured by whole bottle Winkler titration of 125 ml samples using an amperometric method [*Culberson et al.*, 1991] for detecting the triiodide ion reaction end points. Nutrient samples were stored in acid-washed Nalgene™ 60 ml HDPE bottles at −20°C until analyzed using standard colorimetric methods as adapted for autoanalyzers [*Atlas et al.*, 1971; *Gordon et al.*, 1995]. The POC/PN water samples (1–1.5 L) were immediately filtered through precombusted (at 400°C for 4 h) 25 mm Whatman™ GF/F filters. These filters were frozen at sea then later exposed to acid fumes in the laboratory for 24 h to remove inorganic carbon. Dried filters were analyzed using a Carlo Erba NA-1500 elemental analyzer [*Verardo et al.*, 1990].

[24] Sediment cores (∼50 cm long) were recovered with a frame-mounted hydraulically dampened gravity corer designed to sample sandy sediment without pore water drainage and with little disturbance to the sediment-water interface. The acrylic core tubes (ID 10.5 cm) were 94 cm in length, and sediment cores were retained by a spring-loaded-, "core-catcher-," PVC disk that supported an O-ring seal against the tube walls. A compressed air-powered core extruder was used in a refrigerated van (8°C ± 2°C) to extrude the sediments. For some cores, samples were collected in 1 cm

(from 0 to 5 cm) and 2 cm intervals (from 5 to 52 cm) that were then subdivided for subsequent analyses. For other cores, only the top ~20 cm was extruded into a 9.5 cm ID, 30 cm long acrylic core tube. This sediment was covered with seawater from the study site and saved for measurements of composite permeability in a shore-based cold room (T = 10°C ± 2°C) using a falling-head permeameter designed after *Rocha et al.* [2005].

[25] Depth profiles of excess ^{210}Pb activity and sediment organic C (SOC) and total N were measured after subsampled sediments were dried at 60°C for approximately 48 h and finely ground by mortar and pestle. Approximately 20 g of prepared sediment was placed in one of two Canberra GL2020RS LEGe planar (2000 mm^2) γ ray detectors and counted for 24 h to determine activities of ^{210}Pb and ^{214}Pb (used to calculate supported ^{210}Pb) from counts at 46.5 and 661.6 keV [*Wheatcroft and Sommerfield*, 2005]. SOC and total N concentrations were measured by automated combustion (Carlo Erba NA1500 Series 2 elemental analyzer) with acetanilide as the calibration standard after carbonates were removed from ground and weighed samples by concentrated HCl fumigation (modified from *Verardo et al.* [1990]). Chlorophyll and phaeopigment concentrations were determined fluorometrically after frozen sediment samples (2 cm^3) were extracted with 90% acetone for 24 h at 4°C in the dark (Turner Designs AU10) [*Strickland and Parsons*, 1972]. Estimates of the weight percent of fines (or weight percent of silt and clay) were determined based on Stokes law of particle-settling velocity. Subsamples (2 cm^3) from each sediment layer were placed in 15 cm^3 BD Falcon conical centrifuge tubes and covered with 3 cm of filtered seawater from bottom water POC collections. After vigorous shaking, each sample was allowed to stand undisturbed for 10 s, the suspension was pipetted off, and suspended particles were collected on a preweighed filter (25 mm Whatman GF/C). This process was repeated until the water appeared clear, usually five times per sample. The filter was then rinsed with deionized water, wrapped securely in foil, and stored in a −80°C freezer. At a later date, filters and the sand fraction remaining in the tubes were dried and weighed.

2.5. Traditional Chamber and Microprofiler Methods for Estimating Benthic Oxygen Flux

[26] During each research cruise, the field plan was to assess benthic O_2 fluxes by three in situ methods: EC, benthic chambers, and microelectrode profiles. Thus, two additional landers were used in conjunction with BOXER and the hydrographic measurements. Not all lander deployments recovered useful data. The benthic chamber lander was deployed as a free vehicle with releasable ballast. This lander inserted a pair of 20.3 × 20.3 cm box-shaped stainless steel chambers into the sediment. Each Teflon-lined benthic chamber was equipped with an Aanderaa model 4330 O_2 optode and eight spring-actuated syringes for withdrawing time series water samples. The optode's output (0–5 V) was recorded every 5 min by the control electronics for the lander. Flux chambers were gently stirred by a 4 cm × 1 cm Teflon stir bar supported under the lid and driven by a magnetically coupled motor at about 1 Hz. Further, description of the flux chambers are given by *Devol and Christensen* [1993] and *Holcombe et al.* [2001]. Deployment times varied from 12 to 14 h, including delays between landing, chamber implantation, and lid closure.

[27] The microprofiler was mounted at the center of a simple aluminum-frame tripod lander (1.5 m pod center to pod center by 1.6 m high) which was deployed in the same way as BOXER. This microprofiler has channels for four O_2 microelectrodes and a four-wire resistivity sensor [*Reimers and Glud*, 2000]. The sensors were mounted in silicone-oil-filled holders screwed down onto a slotted anodized aluminum ring and connected by cables to a controlling electronics package. During this study the microprofiler was programmed to move the sensors vertically in steps of 0.125 mm, to wait 4 s at each position, then to record from each sensor five readings that were later averaged. Oxygen microelectrodes (Unisense Ox-25) were calibrated assuming a linear slope and two calibration points: an average bottom water reading from 5 to 10 mm above the sediment-water interface and an average background reading in anoxic subsurface sections of the sediment. Only two O_2 microelectrodes were used on most deployments because of a high rate of microelectrode breakage during these cruises (attributed to the activities of Dungeness crabs seen often in sea bottom photos). The resistivity sensor was made by embedding a four-conductor copper ribbon cable in epoxy within a plastic tube and then beveling the tip into the shape of a wedge to expose the wires along a 6 mm wide leading edge. It had a depth resolution of the order of 2 mm and thus began to detect a change in resistance before encountering the sediment-water interface [*Martin et al.*, 1991]. Resistivity measurements in the sediment were converted to the sediment formation factor F by dividing each measurement by an average resistivity reading in the bottom water.

3. Results

3.1. Water Column and Eddy Correlation Measurements

[28] Hydrographic measurements made to coincide with the different lander deployments showed hypoxic conditions (O_2 < 64 μM or 1.43 ml/L) in the bottom waters of the midshelf region of the Oregon coast in both June and August 2009. These waters were also nutrient and particle rich with T, S, and σ_θ ranges of 7°C–8°C, 33.84–33.92, and 26.4–26.6 kg m^{-3}, respectively, properties characteristic of the bottom mixed layer (Table 1 and Figure 3) [*Perlin et al.*, 2005]. EC measurements were made successfully at the NH and HH sites in June and the SH site in August. These measurements occurred over 11–15 h (Figures 4–6). Changes in water properties on these time scales can be attributed largely to cross-shelf motion of bottom waters in response to tidal forcing and changes in upwelling conditions [*Perlin et al.*, 2005]. Long-period O_2 variations were greatest within the SH record and were measured by both the EC microelectrode and independent optode (Figure 5). A pronounced bottom nepheloid layer was evident in June at both the SH and HH sites. The layer was detected by beam transmissivity values <60% near the seafloor and elevated concentrations of POC and PN (Table 1). After clipping problematic intervals from the EC records of Figures 4–6 (e.g., unusually large vertical velocities in the SH data set 72 to 75 min into the record), 94%, 99.5%, and 91% of the data remained for analysis for NH, SH, and HH, respectively.

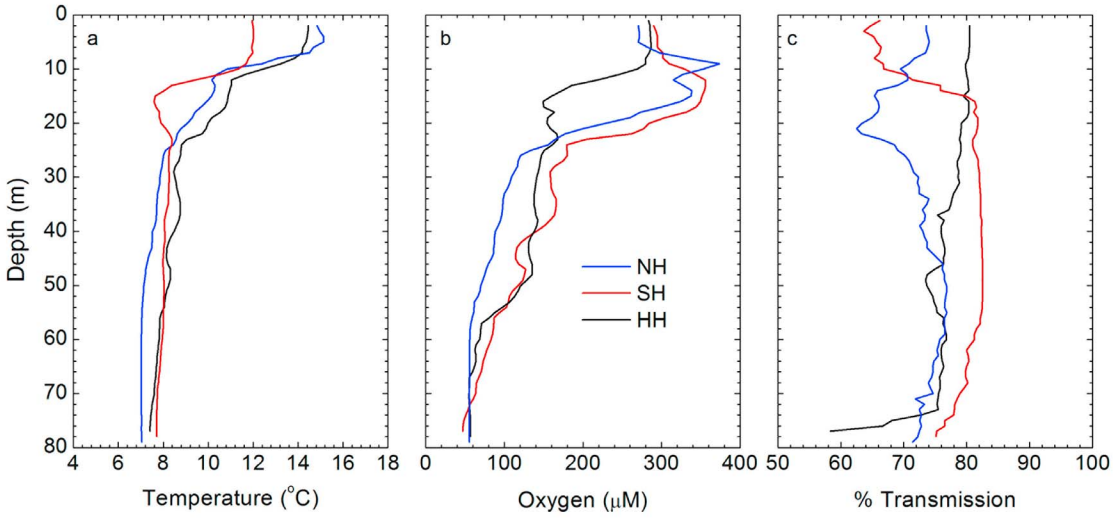

Figure 3. Water column profiles of (a) temperature, (b) dissolved O_2, and (c) percent transmission from the three study sites. The casts displayed coincide with BOXER deployments.

3.2. Effects of Detrending Methods on Eddy Flux Determinations

[29] As noted earlier, different computational and coordinate frame rotation methods are in common use in atmospheric eddy flux studies, and these same methods are available when investigating benthic boundary layer fluxes. Of major concern is how to separate low-frequency oscillations that may bias flux calculations from those that contain significant flux contributions [*Finnigan et al.*, 2003]. In addition, a unique problem in benthic studies is how to consider variable surface and internal wave motions that can dominate the turbulence-induced component of the measured covariance [*Shaw and Trowbridge*, 2001].

[30] The impact of detrending methods to isolate eddy components was first evaluated without any coordinate rotation. In Figure 7a, mean Oregon shelf eddy fluxes calculated after applying a RA filter to every burst period are normalized to the mean flux calculated from the same data after LD. The normalized flux is shown as a function of the RA filter period, which was increased from 0.5 to 14 min. The outcome is different between data sets. The normalized flux curve from site SH flattens near 1.0 when a 3 min or

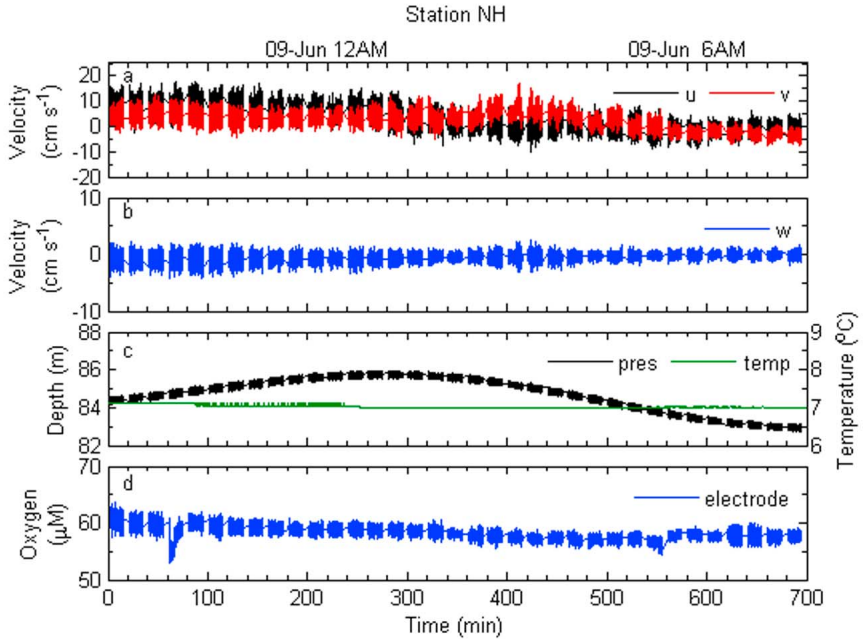

Figure 4. The full EC time series from station NH: (a, b) velocity, (c) pressure, and (d) oxygen microelectrode data are reduced to 16 Hz. Temperature data (also in Figure 4c) from the MK-9 are at 0.067 Hz with a resolution of ±0.05°C.

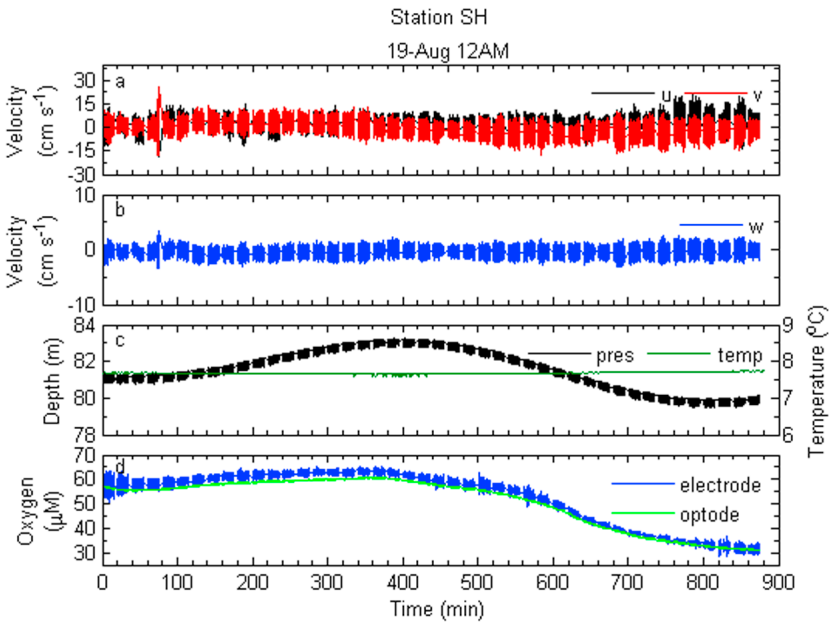

Figure 5. The full EC time series from station SH. The Unisense controller system with optode was used during this deployment. (a, b) Velocity, (c) pressure, and (d) oxygen microelectrode data are reduced to 16 Hz. Optode oxygen measurements (in Figure 5d) are at 1 Hz, and temperature readings from the Mk-9 sensor (in Figure 5c) are at 0.017 Hz.

longer RA filter is applied, but the curves from NH and HH generally increase. This shows that detrending by LD will often give larger-magnitude overall flux estimates until the RA period approaches the length of the data burst.

[31] Both the RA and FF detrending methods indicate greater flux contributions at frequencies <0.005 Hz within the NH and HH data sets compared with SH (Figures 7a and 7b). Cumulative cospectra of $\overline{w'c'}$ examined on a burst-by-burst basis show that contributions to eddy fluxes at frequencies <0.005 Hz are fairly persistent at HH and NH but arise more intermittently within the record from SH. Oscillations occurring on time scales of a few minutes to tens of minutes are consistent with packets of nonlinear internal waves that are geographically and temporally variable sources of turbulent mixing on the Oregon shelf [*D'Asaro et al.*, 2007]. Nonlinear internal waves have large amplitudes and may travel long distances across the shelf, causing a net cross-shelf transport of particles [*Bogucki and*

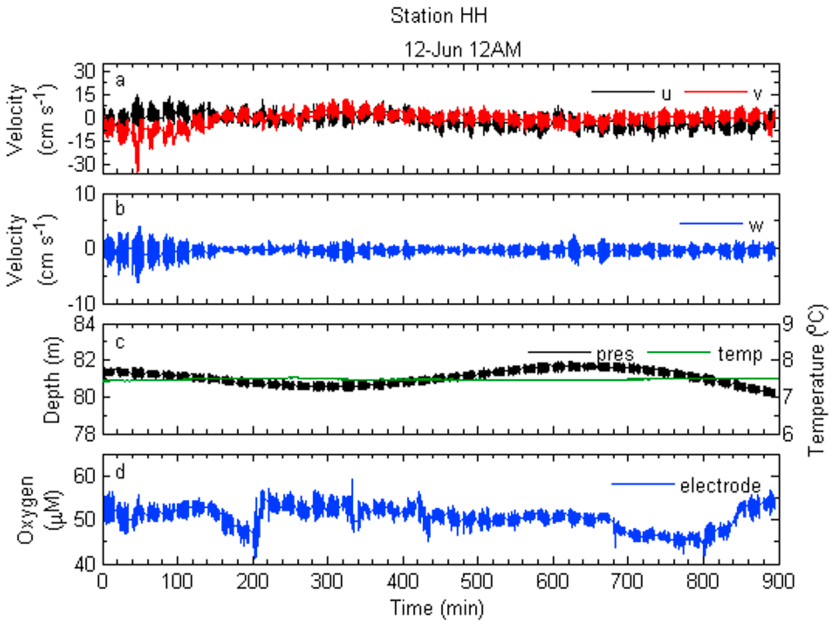

Figure 6. Same as Figure 4 except the data are for HH.

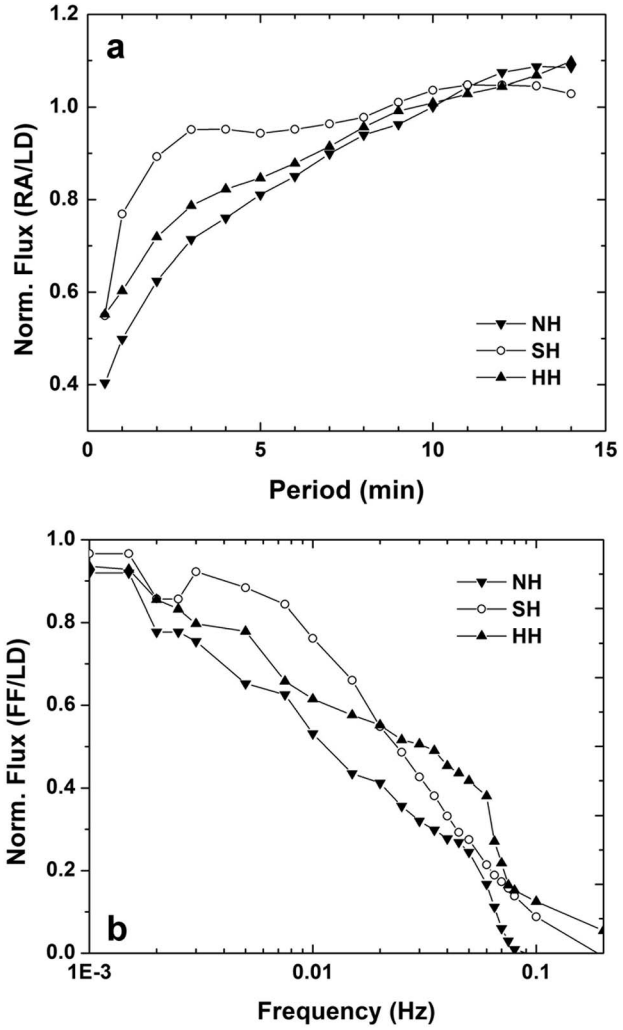

Figure 7. (a) Average fluxes derived after detrending using a centered running average (RA) with increasing filter period normalized to the flux derived after linear detrending (LD). (b) Fluxes after applying a low-pass frequency filter (FF) of increasing cutoff frequency normalized to the flux derived after LD. Each point represents an average from all data bursts after removing some anomalous data segments and without rotation of axes (see text).

Redekopp, 1999]. These phenomena may also explain why in some bursts the lower-frequency portion of cospectra reduces rather than enhances the overall eddy flux estimate of O_2 consumption, and this makes the outcome very sensitive to detrending methods. An example is illustrated by data from 440.5 to 455 min into the HH time series. The eddy flux derived from this data segment equals −2.85, −7.8, −8.6, or −9.2 mmol m^{-2} d^{-1}, depending on whether detrending is by LD, 0.002 Hz FF, 8.33 min RA, or 4 min RA computations, respectively (Figure 8, curve set 1). In contrast, for the burst from 280.5 to 295 min, the same series of fluxes equals −22.4, −12.5, −16.8, and −13.1 mmol m^{-2} d^{-1}, in part because oscillatory trends in this data segment appear to have a period greater than the burst duration (Figure 8, curve set 2).

[32] Figure 8 also illustrates the cutoff behavior of the FF in comparison with other detrending methods in nonrotated data from HH. As frequency contributions approaching 0.001 Hz are both negative and positive in these records, it may be advantageous for there to be a long time series over which these effects will tend to average out. This could be accomplished in the future by having much longer bursts or here by averaging over many bursts. Selecting only a few 10–15 min bursts to represent overall eddy fluxes could misrepresent the strength of the seafloor sink in this environment. These points will be returned to below.

3.3. Coordinate Rotation Influences

[33] A consistent pattern in these EC data sets is that $\overline{w}$ is nonzero and negative (Table 2). Possible causes for this are instrument leveling errors that introduce horizontal flow contributions into w [*Pond*, 1968; *Shaw and Trowbridge*, 2001], complex flow patterns that cause short-term ensembles of mean velocity vectors to orient at an angle relative to the seabed [*Finnigan et al.*, 2003], flow deflection by components of the BOXER framework or sensor supports, or ripple- or other permeable bed form-induced effects on the near-bed velocity field under waves [*Doering and Baryla*, 2002]. Since the Vector contains a compass and tilt meter, these measurements show that the greatest measure of instrument pitch or roll was 4.1° at NH, but these angles were <0.5° at SH and HH. Assuming a nearly level seabed, this implicates complex flow, frame interference, and/or bed form effects at these stations. The practice of rotating coordinates so that $\overline{v_R} = \overline{w_R} = 0$ over each burst is arguably best suited for cases in which there is an instrument leveling error or steady flow at an angle relative to the bottom boundary and has been used by *Berg and Huettel* [2008] and *Berg et al.* [2009]. Rotation results from all three sites show that this rotation method can both increase and decrease apparent fluxes on a burst-by-burst basis. At stations NH and SH, the overall effect is to decrease the magnitude of the average eddy flux (e.g., 53%–61% compared with nonrotated with LD), whereas at HH the magnitude is enhanced (52% compared with nonrotated with LD) and the range for all bursts is greatly expanded (Table 3).

[34] *Finnigan et al.* [2003] suggest that in situations with long-period fluctuations, a complication of rotating coordinates every period is an introduction of horizontal components into $\overline{w'c'}$ rather than their removal. This seems especially likely if the forced rotation angle in the vertical (i.e., around the horizontal axis) is larger than a few degrees as it became for most individually rotated bursts (e.g., at HH the range was −28.2° to −2.6° with a mean of −6.6°). One also sees an enhanced surface wave signal in w_R when such rotated time series are plotted on top of nonrotated data (not shown). These analyses cause us to reject this method of rotating coordinates every period as appropriate for benthic EC measurements of this nature.

[35] Alternatively, a single rotation defined by the requirement that $\overline{v_R} = \overline{w_R} = 0$ only over an entire long-term data record could be applied to fix a new coordinate frame. Such a rotation scheme is best applied when there is a strong current from one direction. Nonetheless, we have done this for the three Oregon shelf data sets, and the effect is much the same, with rotation angles in the vertical of

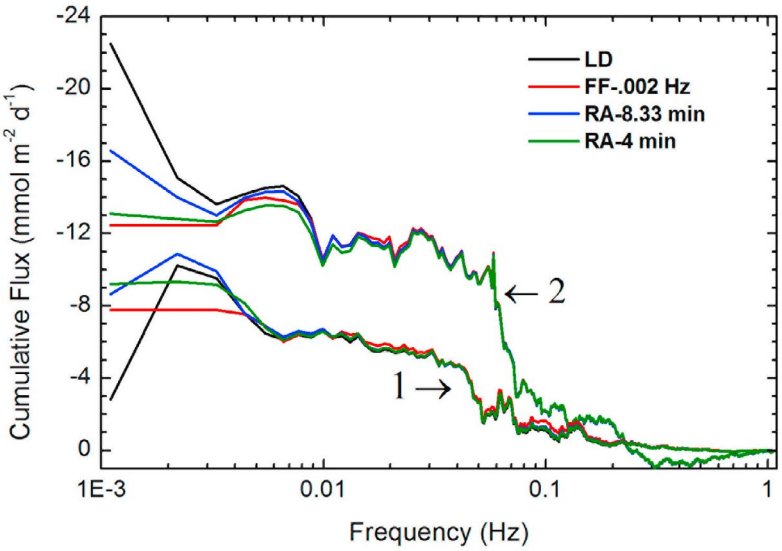

Figure 8. Cumulative cospectra of $w'c'$ from HH data segments spanning 440.5–455 min (point 1) and 280.5–295 min (point 2), computed with $df = 0.0011$ Hz, no rotation of axes, and with linear, low-pass filter (cutoff = 0.002 Hz), or running average (periods = 4 and 8.33 min) detrending methods.

$-10°$ to 16° and most bursts showing an enhanced wave signal in w_R.

[36] Instead, what seems most appropriate is to rotate the coordinates using information extracted from u, v, w and the pressure signal to minimize any wave bias in w_R (as described in section 2.3). The resulting θ_V angles are small, vary little from burst to burst ($-2.1° \pm 0.7°$, $-1.5° \pm 2.9°$, and $0.9° \pm 0.6°$ for NH, SH, and HH, respectively), and are close to the compass angles. The highest variability is observed at SH, where the horizontal rotation angle varies also, likely because of the turbulent nature of the velocities (also see section 3.4). A comparison of eddy fluxes derived with and without this final rotation is presented in Table 3. As rotation effects are not independent of detrending, fluxes predicted after this rotation are also compared with LD, RA, and FF methods. We highlight the combination of linear detrending with the rotation to minimize wave biasing as the "preferred" to represent the strength of the seafloor sink because with these ~15 min burst segmented data sets this treatment both retains more low-frequency contributions within the eddy flux (i.e., last term of equation (2)) and minimizes wave contamination. In effect, we are making the judgment that because data bursts were <15 min and separated by 5 min gaps in time, the best method to retain real wave fluctuations with periods of several minutes to hours is with linear detrending. If the data had been collected in longer bursts or a long-duration continuous mode instead, a low-pass frequency filter would probably be preferable because it could be adjusted to precisely remove very low frequencies (e.g., <~0.0001 Hz; in other words, fluctuations due to long-period exchanges such as tides).

[37] Figure 9 shows the burst-to-burst variability of the preferred flux estimates, reflected as ±1 standard deviation (SD) in Table 3. Cumulative averages in Figure 9 illustrate that several hours of measurements are needed to approach a consistent flux estimate. The drivers of the apparent variability on shorter time scales are discussed in section 4.

3.4. "Real" Surface Wave Contributions to Eddy Fluxes

[38] The significant wave heights (H_{sig}) and average wave periods (T_p) derived from the pressure records of each EC time series were typical for late spring and summer conditions (Table 2). Surface wave observations from the National Data Buoy Center (NDBC) buoy off Newport (buoy 46050) indicate that during the HH deployment, waves were small (significant wave height $H_{sig} \sim 0.8$ m), and the waves were characterized by swell (peak period $T_p \sim 16$ s) from the southwest. Similar waves were present during the NH deployment; however, in addition, NDBC data also give an indication of a secondary sea peak at around an 8 s period. In contrast, during the SH deployment, short-period waves ($T_p \sim 8$ s) were dominant, and associated wave heights were larger ($H_{sig} \sim 2$ m) and approaching from the northwest.

Table 2. Means ±1 SD (Minimum to Maximum) of Vertical and Horizontal Velocities (cm s^{-1}) and Wave Conditions Derived Over Each Data Burst and Averaged Across All Bursts[a]

Site	Number of Bursts	Mean Vertical Velocity $\bar{w}$	Mean Velocity[b] (cm/s)	H_{sig} (m)	T_p (s)
NH	35	-0.51 ± 0.30 (-0.98 to $+0.03$)	5.8 ± 2.7 (0.3 to 10.4)	0.45 ± 0.03	13.9 ± 1.6
SH	44	-0.40 ± 0.19 (-0.83 to $+0.04$)	3.8 ± 1.2 (0.8 to 6.7)	0.44 ± 0.10	11.1 ± 1.2
HH	45	-0.39 ± 0.17 (-1.05 to -0.12)	4.1 ± 2.5 (0.3 to 13.4)	0.60 ± 0.08	15.3 ± 0.9

[a]Significant wave heights (H_{sig}) and periods (T_p) reflect only those surface waves sensed near the seafloor.
[b]Absolute value of resultant of u, v, and w at measuring height above bottom of Vector.

Table 3. Comparison of the Effects of Coordinate Frame Rotation (Each Period) and Mean Removal Method on O_2 Eddy Fluxes Derived From Measurements in This Study[a]

Site and Number of Bursts	Rotation	Mean Removal	Total Eddy Flux ($\overline{w'c'}$)	Wave Frequency Eddy Flux
NH, n = 33	none	LD	−4.4 ± 3.1	−1.26 ± 0.99
	$\overline{v_R} = \overline{w_R} = 0$	LD	−1.7 ± 3.5	−0.69 ± 1.15
	Minimize wave bias	LD	**−3.2 ± 3.2**	**−0.53 ± 0.94**
	Minimize wave bias	RA (8.33 min)	−3.0 ± 3.2	−0.53 ± 0.95
	Minimize wave bias	RA (4 min)	−2.4 ± 2.5	−0.53 ± 0.95
	Minimize wave bias	FF (0.002 Hz)	−2.4 ± 3.0	−0.53 ± 0.99
	Minimize wave bias	FF (0.005 Hz)	−1.9 ± 2.5	−0.53 ± 0.99
SH, n = 44	none	LD	−4.3 ± 4.1	−0.53 ± 0.74
	$\overline{v_R} = \overline{w_R} = 0$	LD	−2.0 ± 6.3	−0.37 ± 0..90
	Minimize wave bias	LD	**−3.9 ± 3.9**	**−0.52 ± 0.65**
	Minimize wave bias	RA (8.33 min)	−3.8 ± 3.6	−0.52 ± 0.65
	Minimize wave bias	RA (4 min)	−3.7 ± 2.9	−0.52 ± 0.65
	Minimize wave bias	FF (0.002 Hz)	−3.4 ± 4.6	−0.53 ±0.68
	Minimize wave bias	FF (0.005 Hz)	−3.5 ± 3.4	−0.53 ±0.68
HH, n = 42	none	LD	−13.0 ± 16.2	−4.1 ± 4.3
	$\overline{v_R} = \overline{w_R} = 0$	LD	−19.8 ± 32.5	−12.2 ± 17.6
	Minimize wave bias	LD	**−9.8 ± 14.9**	**−2.3 ± 3.8**
	Minimize wave bias	RA (8.33 min)	−10.0 ± 13.5	−2.3 ± 3.8
	Minimize wave bias	RA (4 min)	−8.7 ± 11.6	−2.3 ± 3.8
	Minimize wave bias	FF (0.002 Hz)	−9.0 ± 12.1	−2.3 ± 3.8
	Minimize wave bias	FF (0.005 Hz)	−8.1 ± 10.6	−2.3 ± 3.8

[a]All fluxes are burst averages in mmol m^{-2} d^{-1} (±1 SD to reflect the variability between individual bursts that is due to the flow dynamics). Here 6% of the record from NH, 0.5% from SH, and 9% from HH were excluded from these analyses for reasons given in the text. Boldface values are preferred for reasons given in the text. LD, linear detrending; RA, running average filter; FF, a low-pass frequency filter.

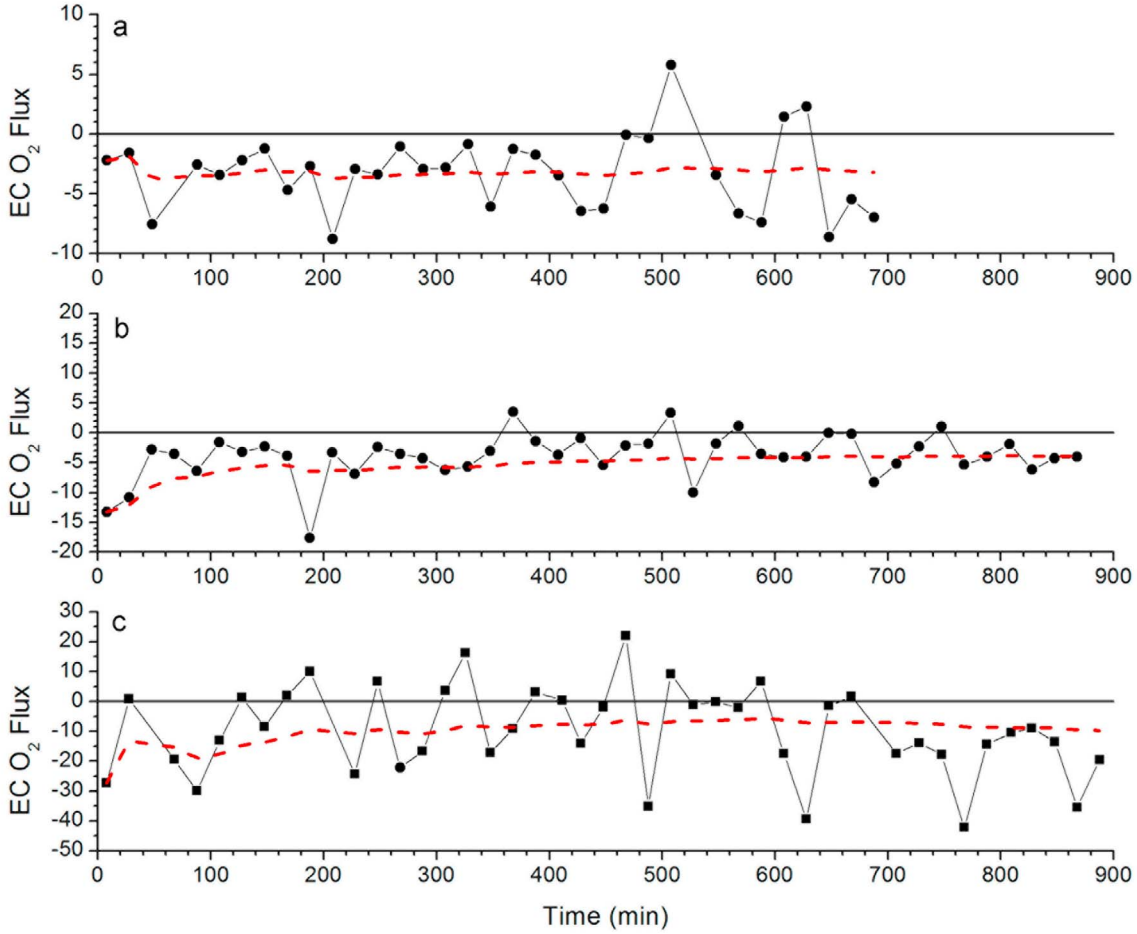

Figure 9. Eddy fluxes of O_2 (mmol m^{-2} d^{-1}) by burst at (a) NH, (b) SH, and (c) HH. These estimates were derived after rotating coordinates to minimize wave biasing and using linear detrending. The dashed red lines represent averages accumulated with increasing number of bursts.

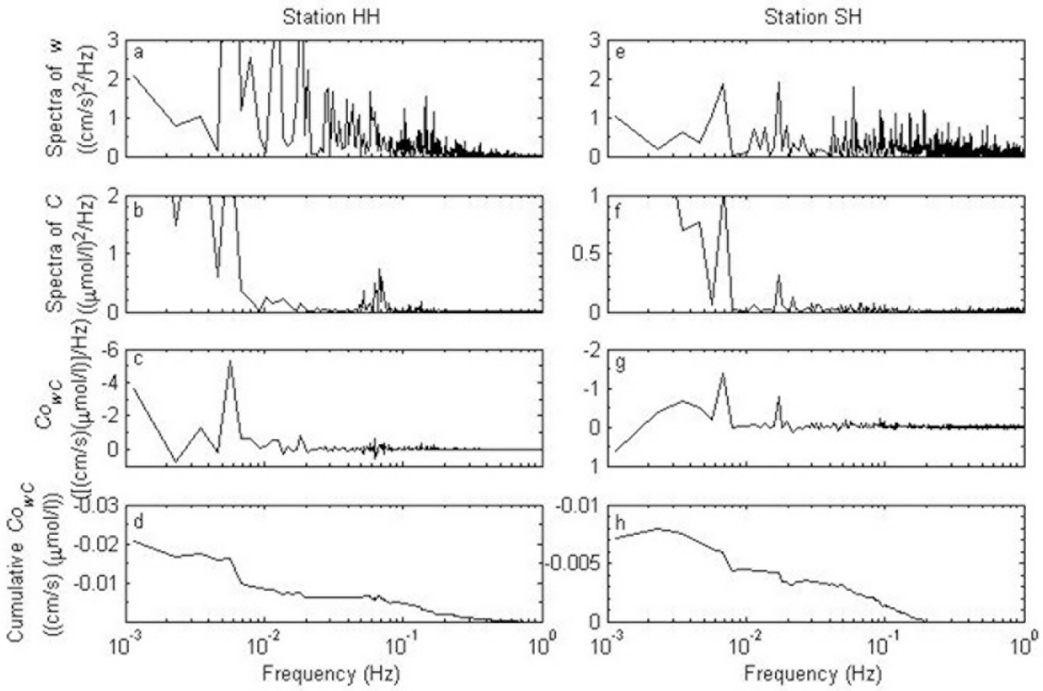

Figure 10. (a, e) Power spectra of vertical velocity w, (b, f) O_2 concentration C with (c, g) cospectra of $w'C'$, and (d, h) cumulative cospectra of $w'C'$ from representative EC data bursts from stations HH and SH. The HH example is from the deployment time interval 740.5–755 min, and the SH example is from 300.5 to 315 min.

However, at the water depth of the EC measurements (80–85 m), waves shorter than approximately 10 s cannot be observed because of the depth attenuation associated with surface gravity waves.

[39] The EC observations show that during the HH (and NH) deployments, oscillations transferred from passing surface waves are most pronounced in u and v. Horizontal velocities derived from the pressure observations are consistently in good agreement with the measured velocities (r^2 values of 0.9 and 0.8 for HH and NH, respectively), indicating that the observed motions are indeed mostly associated with surface gravity waves, with the remaining energy likely due to turbulent motions. Signals associated with the surface gravity waves are also visible in O_2 time series. Oscillations were much less sinusoidal during the SH deployment, and this is apparent in spectral analyses (Figure 10). The observed motions at wave frequencies at SH do not appear as organized swell with a clear propagation direction (r^2 values between pressure-derived velocities and observations were only 0.2, with an equally large standard deviation from burst to burst). Further, frequency spectra derived from the pressure observations clearly indicate that the peak wave frequency cannot be captured because the waves are much shorter during this deployment and hence cannot be observed at these water depths. Instead, the motions measured during the SH deployment are likely primarily due to turbulence, leading to relatively large amplitude fluctuations in w. Without rotation, contributions to total fluxes at NH and HH are clearly heightened at wave frequencies (Figure 7b). After rotation to remove wave biases, the contributions from the dominant surface wave frequency bands to the total EC oxygen fluxes are reduced but still equal to a significant 13%–23% overall (Table 3). These were calculated over a 0.05 Hz frequency band centered at $1/T_p$ (as in Table 2). Mean currents were variable in direction with speeds of <14 cm/s (Table 2).

3.5. Comparability of Eddy Fluxes With Chamber and Microprofile Methods

[40] Confidence in the validity of equating eddy fluxes to the seafloor sink for O_2 can best be obtained by comparison with established benthic flux methods and by considering the relative strengths and weakness of all methods. In this study we were successful in determining alternative estimates of the benthic O_2 flux by deploying a benthic chamber lander and a microprofiler lander at both NH and SH, although contemporaneous measurements by all three methods were achieved only at SH in August (Table 4). Results of side-by-side chamber incubations over 10 h at SH (Figure 11b) show variant trends, but when the sediment uptake of O_2 is estimated from linear fits over the first 180 min, the chamber fluxes are equal to -4.6 ± 0.5 and -7.2 ± 0.7 mmol m^{-2} d^{-1} in June and August, respectively. NH chamber fluxes measured in August were more consistent between chambers (Figure 11a) and equal to -5.8 ± 0.2 mmol m^{-2} d^{-1} (Table 4).

[41] Water-sediment profiles measured in situ at NH and SH with O_2 microelectrodes and a resistivity sensor are shown in Figure 12. Although there is only a single O_2 profile for each deployment (due to either companion sensor breakage or poor-quality records), we have measured similar profiles at other Oregon shelf stations (C. E. Reimers,

Table 4. Summary of Lander Deployments and Coring Stations From Which Data and Comparative Oxygen Fluxes Are Reported

Site	Collection Date, Time, and Type[b]	Position		Water Depth (m)	Total or Diffusive Oxygen Flux (mmol m^{-2} d^{-1})
		Latitude (°N)	Longitude (°W)		
NH	7 Jun 2009, 1921, IMP	44° 39.042′	124° 17.722′	82	−1.1
NH	8 Jun 2009, 1959, BOXER	44° 39.097′	124° 18.005′	82	−3.2 (see Table 3)
HH	11 Jun 2009, 1533, BOXER	43° 55.800′	124° 14.705′	80	−9.8 (see Table 3)
SH	13 Jun 2009, 1458, Chambers	44° 14.033	124° 18.924	82	−4.6 ± 0.5 (n = 2)
SH	18 Aug 2009, 1600, BOXER	44° 14.511′	124° 18.930′	81	−3.9 (see Table 3)
NH	20 Aug 2009, 1843, Chambers	44° 39.398′	124° 18.006′	82	−5.8 ± 0.2 (n = 2)
NH	20 Aug 2009, 2022, IMP	44° 39.099′	124° 17.750′	81	−2.7
SH	21 Aug 2009, 1700, Chambers	44° 14.701′	124° 18.896′	81	−7.2 ± 0.7 (n = 2)
SH	21Aug 2009, 1922, IMP	44° 14.515′	124° 18.871′	81	−2.4

Site	Collection Date, Time, and Type[b]	Position		Water Depth (m)	Permeability or Sampling History
		Latitude (°N)	Longitude (°W)		
NH	7 Jun 2009, 1501, Corer	44° 38.940′	124° 18.000′	83	sectioned into 1 and 2 cm intervals
NH	7 Jun 2009, 1518, Corer	44° 38.949′	124° 18.001′	83	1.74 (±0.09) × 10^{-11} m^{2a}
SH	18 Aug 2009, 1636, Corer	44° 13.321′	124° 19.047′	81	1.76 (±0.08) × 10^{-10} m^2
SH	18 Aug 2009, 1653, Corer	44° 13.321′	124° 19.049′	81	sectioned into 1 and 2 cm intervals
HH	11 Jun 2009, 1936, Corer	43° 56.094′	124° 14.994′	81	sectioned into 1 and 2 cm intervals

[a]Four replicate measurements of permeability were made per core. Uncertainties represent ±1 SD.
[b]Time given as local time.

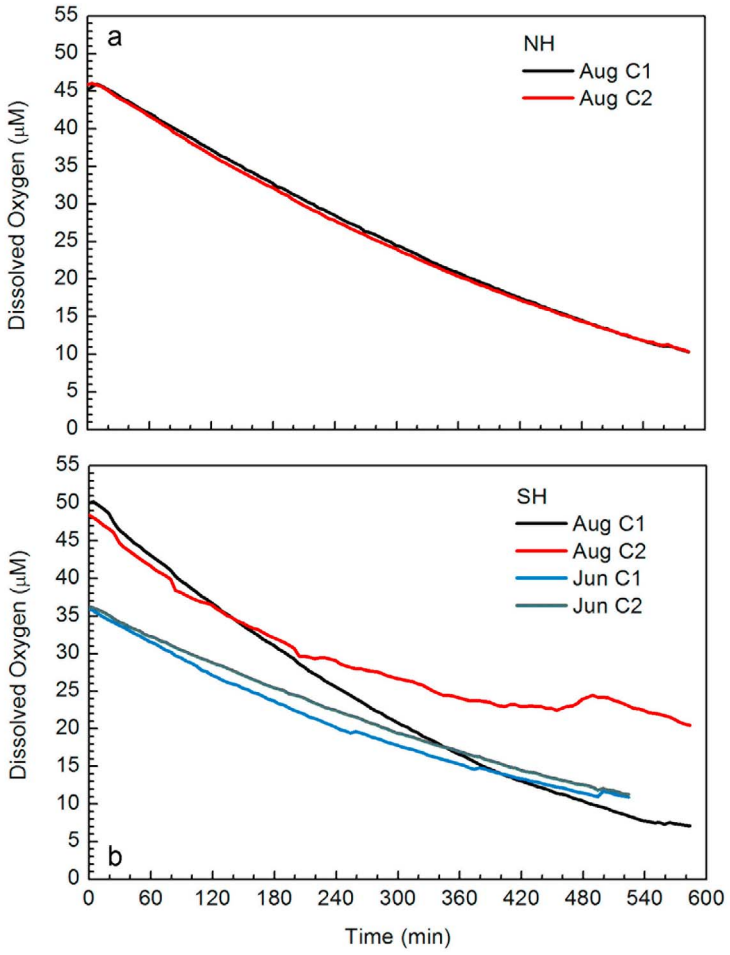

Figure 11. Dissolved oxygen concentration versus time in benthic chambers during NH and SH deployments. C1, chamber 1; C2, chamber 2. Oxygen was measured by optodes mounted in the chamber lids. These records start at the time of chamber closure, which occurred 3–5 h after deployment. Chamber fluxes are derived from linear fits to the O_2 consumption over the first 180 min.

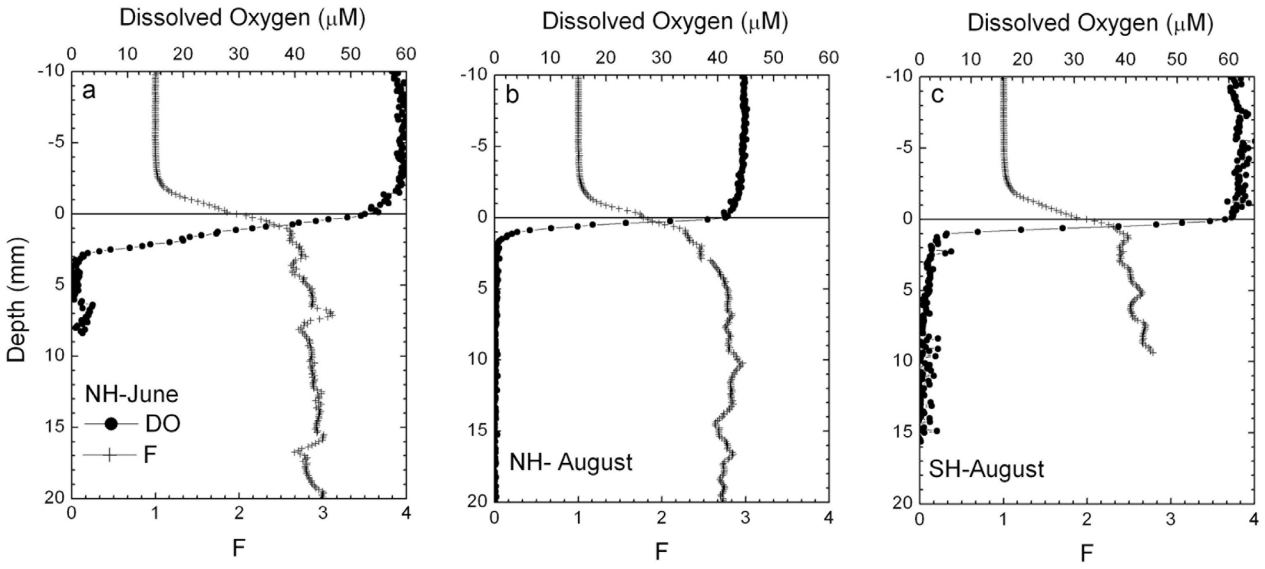

Figure 12. Profiles of O_2 and sediment formation factor measured in situ at (a) NH in June, (b) NH in August, and (c) SH in August 2009.

unpublished data, 2009), and so have confidence that these are typical for summer hypoxic conditions. The steep interfacial gradients do not indicate any deep O_2 intrusion due to flow- or wave-induced advection and can be used with Fick's first law as it is often applied to sediments: $\mathrm{DOU} = -\frac{D_o}{F}\frac{\partial C}{\partial z}$, where D_o is the molecular diffusion coefficient for O_2 at in situ temperatures and F is the formation factor of interfacial sediment [*Ullman and Aller*, 1982; *Schulz*, 2006] to derive diffusive O_2 fluxes equal to -1.1, -2.7, and -2.4 mmol m^{-2} d^{-1} at NH in June, NH in August, and SH in August 2009, respectively (Table 4). However, we fully expect DOU calculations to underestimate the total flux. As demonstrated by *Güss* [1998], purely hydrodynamic dispersion can enhance the O_2 uptake near the interface of permeable sediments by several times molecular diffusion without much deepening of the O_2 penetration. These potential effects, in addition to respiration of macrofauna and biological pore water irrigation, imply that both the EC and chamber oxygen fluxes are realistic representations of total oxygen consumption rates.

3.6. Sediment Properties Driving Variability in Eddy Fluxes

[42] The most striking variability in average eddy fluxes derived for the three shelf sites is the greater flux at HH compared with the two sites further north. As water depth, bottom water O_2 concentrations, and temperature were largely consistent during these three deployments and wave conditions were similar between HH and NH, we look to the sediments for another source of the variability. The collection information for sediment cores that were analyzed for this study is presented in Table 4 with measurements of composite permeability (sites NH and SH only). Profiles of sediment properties downcore are displayed in Figure 13. There is little to distinguish the HH site except for its relatively higher percentages of fines and organic carbon content. Concentrations of excess ^{210}Pb are low at all sites (especially in comparison with shelf muds) and indicate that the top ~7 cm of the three sites have comparable histories of winnowing and bioturbation. Chlorophyll-*a* is generally enriched at the sediment surface, but chlorophyll-to-phaeophytin molar ratios (averaging 0.31 ± 0.12 and not shown) change little with sediment depth or between cores.

4. Discussion

4.1. Assessment of Fluxes

[43] Although the derivation of benthic fluxes from EC measurements may be described in straightforward steps [e.g., *Kuwae et al.*, 2006; *Lorrai et al.*, 2010], in practice this study shows that not all data sets are simple, and the outcome from EC can be sensitive to the methods used to orient coordinates and split measurements into mean and fluctuating components. On the Oregon continental shelf, because velocities were dominated by wave motions rather than by currents and because measurements were made in a relatively short burst mode, we find that the most defendable fluxes are derived by (1) orienting the coordinate axes to minimize surface wave biasing of the vertical velocity and (2) applying linear detrending methods to retain within the eddy contributions the lowest frequencies sampled per burst (0.0011 Hz in this study). This processing does not remove all the flux contributions at surface wave frequencies (as seen in Figure 10 and Table 3), but what remains is inferred to be due to real wave- or pressure-driven exchange processes that transport bottom water enriched in oxygen into at least the uppermost millimeters of a permeable seabed and oxygen-depleted pore water out [*Precht et al.*, 2004]. With relatively short data bursts (<15 min), the longest-period oscillations that may be incorporated into the EC oxygen flux are on the time scales of internal waves, which are known to enhance turbulence on the Oregon continental shelf [*D'Asaro et al.*, 2007]. Bioirrigation may be another mechanism to produce low-frequency components in O_2

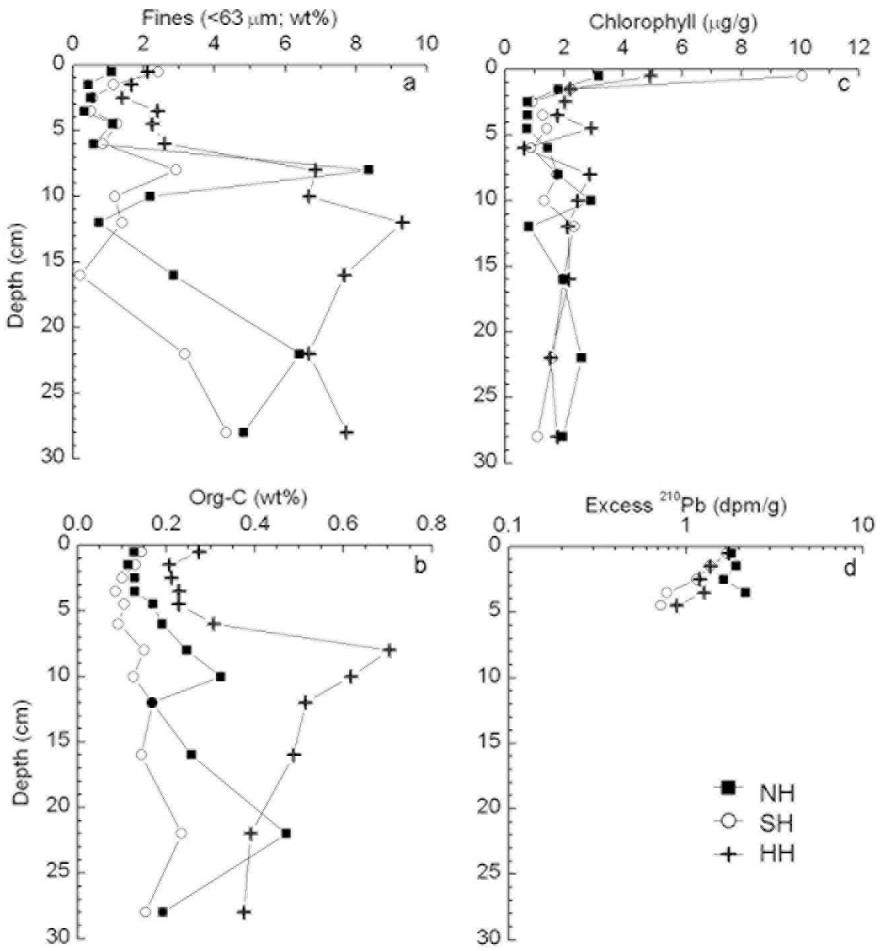

Figure 13. Profiles of sediment properties from cores: (a) wt % fines, (b) wt % organic C, (c) chlorophyll-*a*, and (d) excess ^{210}Pb.

spectra (Figure 10). Low-pass frequency filter analyses with a cutoff frequency of 0.005 Hz when compared with LD (Table 3) indicate contributions at frequencies of <0.005 Hz carried about 41%, 10%, and 17% of total EC oxygen fluxes assessed from the NH, SH, and HH deployments, respectively. In contrast, real contributions at surface wave frequencies were assessed as equal to 17%, 13%, and 23%, respectively (Table 3). This implies that between 42% and 77% of measured eddy fluxes arose from turbulent eddies at typical near-bottom frequencies [*Shaw and Trowbridge*, 2001].

[44] Another important conclusion is that because of low-frequency oscillations, conservation may in fact hold over the course of only a relatively long time series (at least several hours). This means that only when averaged over such long time scales can eddy fluxes correctly represent the seafloor sink. Said in other terms, the sometimes large variability between the eddy fluxes derived for individual bursts (Figure 9) is because internal waves or other low-frequency mixing events cause intermittent advection or flux divergence contributions to continuity [see also *Brand et al.*, 2008; *McGinnis et al.*, 2011]. This reasoning is why we caution readers to be cognizant that the short-term variability of the eddy fluxes as reported in Table 3 is not a measure that should be used to infer whether fluxes are significantly different between sites. In essence, we consider $n = 1$ for each BOXER deployment (Table 4), and the results of replicate deployments are required before statistical tests concerning mean fluxes are attempted.

[45] The smaller magnitudes of the eddy flux assessments of O_2 uptake compared with those of chambers, both of which are greater (as expected) than diffusive flux estimates from O_2 microelectrode profiles, are results that differ from past comparison studies in marine environments with sandy sediments. For example, *Berg and Huettel* [2008] found an average nighttime O_2 uptake assessed by EC to be 3.8 times the rate derived from diver-deployed cylindrical chambers in a shallow (~1 m depth) nearshore site in Apalachicola Bay, Florida. In the Florida study, the three velocity components were rotated so that $w_R \rightarrow 0$ every burst; however, the resulting eddy flux was not highly sensitive to changes in coordinate orientation. We suspect that shallow sites like Apalachicola Bay, which are under nearly air-saturated waters and experience regularly strong tidal currents, exhibit a greater degree of advective oxygen flux enhancement than the ~80 m Oregon shelf sites we have studied under late

spring and summer conditions. Flux contributions due to pore water pumping through a few to tens of centimeters of highly permeable sediment are not easily measured by benthic chambers [*Jahnke et al.*, 2005]. However, more work will need to be done to fully understand the effects of flux methodology, water depth, and physical variables on exchange processes involving such permeable sediments.

[46] In this study, the only contemporaneous comparison of O_2 flux methods was at SH. The observed eddy-to-chamber flux ratio of 0.54 may indicate that the chambers sampled a localized "hot spot" within the Oregon shelf benthos such as has been documented on other margins and ascribed to an inhomogeneous distribution of decomposing phytodetritus [e.g., as in *Glud et al.*, 2009]. Additionally, chamber methods have their own sources of error and biasing. As reviewed by *Reimers et al.* [2001] and *Viollier et al.* [2003], among the potential concerns are (1) changes in the hydrodynamic regime, including the diffusive sublayer adjacent to the sediment surface; (2) artificially inducing or blocking advective pore water flow (especially with permeable sediments); and (3) artifacts caused by chambers disturbing the water and sediment layers to be studied. The chambers used in this study were square and relatively small (0.04 m^2), but have yielded O_2 and silicate fluxes that agreed within a factor of 2 with a wide variety of other designs during an intercalibration study [*Tengberg*, 1997]. *Glud and Blackburn* [2002] argue that insertion of small chambers will, per area of sediment, damage a greater number of fauna and burrows, which could enhance the O_2 flux. These effects should be proportionally greater when overall O_2 fluxes are low. The nonlinear O_2 traces (Figure 11) suggest a changing sediment-water interface gradient as the overlying water concentration decreases and (at SH) some divergent behavior, probably caused by different irrigation or bioturbation rates of benthic fauna.

[47] Our results do show an increase in eddy fluxes at 80 m moving from north off Newport to south off Hecata Head under similar late spring and summer conditions. This latitudinal trend is probably the best evidence that the eddy fluxes are valid representations of benthic O_2 consumption rates in this region. The water column and sediments to the south were observed to be richer in organic carbon, indicating sources of both fresh and buried organic matter to intensify rates of O_2 utilization. A pronounced bottom nepheloid layer was also evident at station HH in June. Cross-shelf motion of these near-bottom layers in response to changes in tides and upwelling-relaxation cycles has been described by *Perlin et al.* [2005], but it is not known how the variable turbulence and particulate loads of these layers couple to benthic biogeochemical cycling. There is an indication that regions of high turbidity are associated with regions of higher turbulence stemming in part from internal waves generated in areas of rough topography [*D'Asaro et al.*, 2007]. *Barth et al.* [2005] describe a low-temperature, high-salinity, turbid bottom water pool, supplied primarily from the south in the lee region inshore of Heceta Bank and speculate that this region could be relatively important in the generation of low-O_2 waters on the shelf through local respiration. Our measurements support this possibility and suggest a need for additional flux measurements in the vicinity and farther south of HH.

4.2. The Contribution of Benthic Oxygen Consumption to Hypoxia

[48] Hypoxia at shelf depths in late spring and summer on the Oregon continental margin is indicated to be a new phenomenon that may signal an ecosystem response to changes in upwelling wind stress from climate warming [*Grantham et al.*, 2004; *Chan et al.*, 2008]. It is debated whether more severe hypoxia has arisen because of a greater contribution of low-O_2 source waters to the shelf or instead from greater in situ drawdown of O_2 through respiration in the benthic boundary layer including the sediments [*Connolly et al.*, 2010]. Encompassing our measurements, current meter and dissolved O_2 records from a moored platform at 70 m adjacent to SH showed that hypoxic conditions persisted in the bottom boundary layer for over two-thirds of the time between mid-April and mid-September 2009 (K. Adams and J. Barth, personal communication, 2011). During the same period, there were four major wind-driven upwelling events followed by intervals of wind relaxation and downwelling. As a consequence, at midshelf depths, cumulative along shore currents were relatively weak, which extended the local residence time of a density-confined bottom boundary layer (K. Adams and J. Barth, personal communication, 2011). Longer residence times of bottom boundary waters on the shelf should facilitate O_2 depletion by the sedimentary sink.

[49] The measurements reported here provide a baseline range for total seafloor O_2 utilization rates of approximately 3 to 10 mmol m^{-2} d^{-1}. Using these rates, benthic respiration can be expected to deplete O_2 at a rate on the order of 1 μM d^{-1} from the bottom 5–10 m of the water column, which matches rates estimated for water column respiration and for sedimentary O_2 consumption from mass balances of dissolved O_2 and nitrate in near-bottom waters by *Connolly et al.* [2010] for the Washington shelf. In the future, we hope to document how sensitive benthic O_2 fluxes are to bottom water O_2 concentrations, water depth, and the internal and surface wave conditions in this region. However, compared with other marine environments of similar water depths [*Glud*, 2008], the benthic O_2 consumption rates measured so far on the Oregon shelf are lower than average (the regression of global data of *Glud* [2008, Figure 16] predicts a typical total O_2 utilization rate = 11 mmol m^{-2} d^{-1} for a depth = 80 m). The relatively low rates suggest that (1) hypoxic conditions create a negative feedback (i.e., lower bottom water O_2 leads to a lower O_2 consumption rate) [*Eldridge and Morse*, 2008] and (2) the recent rise in shelf hypoxia along the U.S. West Coast is not because local respiration rates have increased in response to climate forcing. Rather, shelf hypoxia appears in response to more persistent (but interannually variable) upwelling-relaxation cycles that combine to inject O_2-depleted source waters onto the shelf, then hold these waters in the bottom boundary in contact with the benthic sink for O_2.

5. Summary and Conclusions

[50] This study presents sediment oxygen uptake rates determined from eddy correlation measurements made using a new lander (BOXER) designed for deployments from research vessels and investigations of continental shelf environments. When the lander was applied off central Oregon at ~80 m depth in June 2009, surface wave (swell

with a peak period $T_p \sim 16$ s) impacts on variations in vertical velocities and O_2 were strongly evident, while in August 2009 surface waves were much shorter and hence the variations measured were primarily due to turbulence.

[51] Three detrending methods (linear, centered running average, and low-pass frequency filter) were compared, leading to the assessment that linear detrending is most effective when data bursts are of durations similar to those of important nonturbulent motions such as internal waves. However, if longer data bursts or continuous records are collected in future studies, a low-pass frequency filter set to eliminate long-period fluctuations would have the advantage of more precisely defining the frequencies of dynamic processes included in EC fluxes. Furthermore, records of pressure variations were shown to be useful for establishing coordinate rotation angles that minimize the contamination of vertical velocity components with horizontal components of wave motion.

[52] The EC O_2 fluxes determined ranged between -3 and -10 mmol m^{-2} d^{-1} while benthic chamber O_2 fluxes measured in duplicate at just two of the stations ranged between -4 and -8 mmol m^{-2} d^{-1}. All fluxes are too low to implicate an intensification of local diagenetic processes for a greater prevalence of hypoxic conditions in the benthic boundary layer of the Oregon shelf during the last decade. However, local depletion rates may be sensitive to a number of local variables such as water depth, the dynamics of internal mixing, bottom water O_2, sediment permeability, ripple regime, and sediment organic matter content. It is our intention to examine these controls more comprehensively in future research.

[53] **Acknowledgments.** We thank the officers and crew of the R/V *Wecoma* for ensuring the successful execution of this research. Oregon State University Marine Technicians Daryl Swensen and David O'Gorman contributed greatly to the deployment strategy and provided critical equipment repairs while at sea. We thank Jay Simpkins and Tim Nolan for design and construction of the BOXER lander. Lars Damsgaard, from Unisense A/S, provided dedicated support of the EC equipment and its development for this research. Cody Doolan, Joe Jennings, Margaret Sparrow, Yvan Alleau, and Steve Pierce provided invaluable help with collecting and analyzing the water column and sediment data reported. Wendi Ruef and Bonnie Chang provided technical support of the benthic chambers. Rob Wheatcroft provided use of his lab's gamma ray detectors. Support for this project was provided by the National Science Foundation under grants OCE 0726984 and 1061218 to C. Reimers and is gratefully acknowledged. A. Devol's participation was supported by NSF grant OCE 0628391. The paper was improved after receiving helpful reviews from Richard Dewey, Filip Meysman, Cecile Cathalot, and an anonymous reviewer.

References

Allan, J. C., and P. D. Komar (2006), Climate controls on US west coast erosion processes, *J. Coastal Res.*, *22*, 511–529, doi:10.2112/03-0108.1.

Andersen, K., T. Kjær, and N. P. Revsbech (2001), An oxygen insensitive microsensor for nitrous oxide, *Sens. Actuators B*, *81*, 42–48, doi:10.1016/S0925-4005(01)00924-8.

Atlas, E. L., S. Hager, L. Gordon, and P. Park (1971), A practical manual of use of the Technicon AutoAnalyzer in seawater nutrient analyses, *Rev. Oreg. State Univ. Tech. Rep. 215*, Dept. of Oceanogr., Oreg. State Univ., Corvallis.

Aubinet, M. (2008), Eddy covariance CO_2 flux measurements in nocturnal conditions: An analysis of the problem, *Ecol. Appl.*, *18*(6), 1368–1378, doi:10.1890/06-1336.1.

Barth, J. A., S. D. Pierce, and R. M. Castelo (2005), Time-dependent, wind-driven flow over a shallow mid-shelf submarine bank, *J. Geophys. Res.*, *110*, C10S05, doi:10.1029/2004JC002761.

Barth, J. A., B. A. Menge, J. Lubchenco, F. Chan, J. M. Bane, A. R. Kirinich, M. A. McManus, K. J. Nielsen, S. D. Pierce, and L. Washburn (2007), Delayed upwelling alters nearshore coastal ocean ecosystems in the northern California current, *Proc. Natl. Acad. Sci. U. S. A.*, *104*, 3719–3724, doi:10.1073/pnas.0700462104.

Bendat, J. S., and A. G. Piersol (1971), *Random Data: Analysis and Measurement Procedures*, 407 pp., Wiley-Interscience, New York.

Berg, P., and M. Huettel (2008), Monitoring the seafloor using the noninvasive eddy correlation technique: Integrated benthic exchange dynamics, *Oceanography*, *21*, 164–167, doi:10.5670/oceanog.2008.13.

Berg, P., H. Røy, F. Janssen, V. Meyer, B. B. Jørgensen, M. Huettel, and D. de Beer (2003), Oxygen uptake by aquatic sediments measured with a novel non-invasive eddy-correlation technique, *Mar. Ecol. Prog. Ser.*, *261*, 75–83, doi:10.3354/meps261075.

Berg, P., H. Røy, and P. Wiberg (2007), Eddy correlation flux measurements: The sediment surface area that contributes to the flux, *Limnol. Oceanogr.*, *52*, 1672–1684, doi:10.4319/lo.2007.52.4.1672.

Berg, P., R. N. Glud, A. Hume, H. Stahl, K. Oguri, V. Meyer, and H. Kitazato (2009), Eddy correlation measurements of oxygen uptake in deep ocean sediments, *Limnol. Oceanogr. Methods*, *7*, 576–584, doi:10.4319/lom.2009.7.576.

Bogucki, D., and L. G. Redekopp (1999), A mechanism for sediment resuspension by internal solitary waves, *Geophys. Res. Lett.*, *26*(9), 1317–1320, doi:10.1029/1999GL900234.

Brand, A., D. F. McGinnis, B. Wehrli, and A. Wüest (2008), Intermittent oxygen flux from the interior into the bottom boundary of lakes as observed by eddy correlation, *Limnol. Oceanogr.*, *53*, 1997–2006, doi:10.4319/lo.2008.53.5.1997.

Castelao, R. M., and J. A. Barth (2005), Coastal ocean response to summer upwelling favorable winds in a region of alongshore bottom topography variations off Oregon, *J. Geophys. Res.*, *110*, C10S04, doi:10.1029/2004JC002409.

Chan, F., J. A. Barth, J. Lubchenco, A. Kirincich, H. A. Weeks, W. H. Peterson, and B. A. Menge (2008), Emergence of anoxia in the California Current large marine ecosystem, *Science*, *319*, 920, doi:10.1126/science.1149016.

Chen, C.-T. A., A. Andreev, K.-R. Kim, and M. Yamamoto (2004), Roles of continental shelves and marginal seas in biogeochemical cycles of the North Pacific Ocean, *J. Oceanogr.*, *60*, 17–44, doi:10.1023/B:JOCE.0000038316.56018.d4.

Connolly, T. P., B. M. Hickey, S. L. Geier, and W. P. Cochlan (2010), Processes influencing seasonal hypoxia in the northern California Current System, *J. Geophys. Res.*, *115*, C03021, doi:10.1029/2009JC005283.

Culberson, C. H., G. Knapp, M. C. Stalcup, R. T. Williams, and F. Zemlyak (1991), A comparison of methods for the determination of dissolved oxygen in sea water, *WHP Office Rep. WHPO-91–2*, World Ocean Circ. Exp. Hydrogr. Prog. Off., La Jolla, Calif.

D'Asaro, E. A., R.-C. Lien, and F. Henyey (2007), High-frequency internal waves on the Oregon continental shelf, *J. Phys. Oceanogr.*, *37*, 1956–1967, doi:10.1175/JPO3096.1.

Dean, R. G., and R. A. Dalrymple (1992), *Water Wave Mechanics for Engineers and Scientists*, 353 pp., World Sci., Teaneck, N. J.

Devol, A. H., and J. P. Christensen (1993), Benthic fluxes and nitrogen cycling in sediments of the continental margin of the eastern North Pacific, *J. Mar. Res.*, *51*, 345–372, doi:10.1357/0022240933223765.

Doering, J. C., and A. J. Baryla (2002), An investigation of the velocity field under regular and irregular waves over a sand beach, *Coastal Eng.*, *44*, 275–300, doi:10.1016/S0378-3839(01)00037-0.

Eldridge, P., and J. Morse (2008), Origins and temporal scales of hypoxia on the Louisiana shelf: Importance of benthic and sub-pycnocline water metabolism, *Mar. Chem.*, *108*, 159–171, doi:10.1016/j.marchem.2007.11.009.

Feigenwinter, C., C. Bernhofer, and R. Vogt (2004), The influence of advection on the short term CO_2-budget in and above a forest canopy, *Boundary Layer Meteorol.*, *113*, 201–224, doi:10.1023/B:BOUN.0000039372.86053.ff.

Finnigan, J. J. (1999), A comment on the paper by Lee (1998), "On micrometeorological observations of surface-air exchange over tall vegetation," *Agric. For. Meteorol.*, *97*, 55–64, doi:10.1016/S0168-1923(99)00049-0.

Finnigan, J. J., R. Clement, Y. Malhi, R. Leuning, and H. A. Cleugh (2003), A re-evaluation of long-term flux measurement techniques. Part I: Averaging and coordinate rotation, *Boundary Layer Meteorol.*, *107*, 1–48, doi:10.1023/A:1021554900225.

Glud, R. N. (2008), Oxygen dynamics of marine sediments, *Mar. Biol. Res.*, *4*, 243–289, doi:10.1080/17451000801888726.

Glud, R. N., and N. Blackburn (2002), The effect of chamber size on benthic oxygen uptake measurements: A simulation study, *Ophelia*, *56*, 23–31.

Glud, R. N., H. Stahl, P. Berg, F. Wenhöfer, K. Oguri, and H. Kitazato (2009), In situ microscale variation in distribution and consumption of O_2: A case study from a deep ocean margin sediment (Sagami Bay, Japan), *Limnol. Oceanogr.*, *54*, 1–12, doi:10.4319/lo.2009.54.1.0001.

Glud, R. N., P. Berg, A. Hume, P. Batty, and M. E. Blicher (2010), Benthic O_2 exchange rates across hard-bottom substrates quantified by eddy correlation in a sub-Arctic fjord system, *Mar. Ecol. Prog. Ser.*, *417*, 1–12, doi:10.3354/meps08795.

Gordon, L. I., J. C. Jennings, A. R. Ross, and J. M. Krest (1995) A suggested protocol for continuous flow automated analysis of seawater nutrients (phosphate, nitrate, nitrite, and silicic acid) in the WOCE Hydrographic Program and the Joint Global Ocean Fluxes Study, *Oreg. State Univ. Tech. Rep.93–1*, Oreg. State Univ., Corvallis.

Goring, D. G., and V. I. Nikora (2002), Despiking acoustic Doppler velocimeter data, *J. Hydraul. Eng.*, *128*, 117–126, doi:10.1061/(ASCE)0733-9429(2002)128:1(117).

Grantham, B. A., F. Chan, K. J. Nielsen, D. S. Fox, J. A. Barth, J. Huyer, J. Lubchenco, and B. A. Menge (2004), Upwelling-driven nearshore hypoxia signals ecosystem and oceanographic changes in the northeast Pacific, *Nature*, *429*, 749–754, doi:10.1038/nature02605.

Güss, S. (1998), Oxygen uptake at the sediment water interface simultaneously measured using a flux chamber method and microelectrodes: Must a diffusive boundary layer exist?, *Estuarine Coastal Shelf Sci.*, *46*, 143–156, doi:10.1006/ecss.1997.0265.

Hales, B., L. Karp-Boss, A. Perlin, and P. A. Wheeler (2006), Oxygen production and carbon sequestration in an upwelling coastal margin, *Global Biogeochem. Cycles*, *20*, GB3001, doi:10.1029/2005GB002517.

Holcombe, B. L., R. G. Kiel, and A. H. Devol (2001), Determination of pore-water dissolved organic carbon fluxes from Mexican margin sediments, *Limnol. Oceanogr.*, *46*, 298–308, doi:10.4319/lo.2001.46.2.0298.

Huettel, M., and I. T. Webster (2001), Porewater flow in permeable sediments, in *The Benthic Boundary Layer: Transport Processes and Biogeochemistry*, edited by B. P. Boudreau and B. B. Jørgensen, pp. 144–177, Oxford Univ. Press, New York.

Hume, A. C., P. Berg, and K. J. McGlathery (2011), Dissolved oxygen fluxes and ecosystem metabolism in an eelgrass (*Zostera marina*) meadow measured with the eddy correlation technique, *Limnol. Oceanogr.*, *56*, 86–96, doi:10.4319/lo.2011.56.1.0086.

Jahnke, R. A. (2010), Global synthesis, in *Carbon and Nutrient Fluxes in Continental Margins*, *Intl. Geosphere-Biosphere Prog. Ser.*, vol. 28, edited by K. K. Liu et al., chap. 16, pp. 597–616, Springer, Berlin.

Jahnke, R., M. Richards, J. Nelson, C. Robertson, A. Rao, and D. Jahnke (2005), Organic matter remineralization and porewater exchange rates in permeable South Atlantic Bight continental shelf sediments, *Cont. Shelf Res.*, *25*, 1433–1452, doi:10.1016/j.csr.2005.04.002.

Komar, P. D., R. H. Neudeck, and L. D. Kulm (1972), Observations and significance of deep-water oscillatory ripple marks on the Oregon continental shelf, in *Shelf Sediment Transport: Process and Patterns*, edited by D. J. P. Swift, D. B. Duane, and O. H. Pilkey, pp. 601–619, Dowden, Hutchinson and Ross, Stroudsburg, Penn.

Kulm, L. D. (1978), Coastal morphology and geology of the ocean bottom the Oregon region, in *The Marine Plant Biomass of the Pacific Northwest Coast*, edited by R. Krauss, pp. 9–35, Oregon State Univ. Press, Corvallis.

Kuwae, T., K. Kamio, T. Inoue, E. Miyoshi, and Y. Uchiyama (2006), Oxygen exchange flux between sediment and water in an intertidal sandflat, measured in situ by the eddy-correlation method, *Mar. Ecol. Prog. Ser.*, *307*, 59–68, doi:10.3354/meps307059.

Lee, X., W. Massman, and B. Law (2004), *Handbook of Micrometeorology: A Guide for Surface Flux Measurement and Analysis*, Kluwer Acad., Dordrecht, Netherlands.

Lorrai, C., D. F. McGinnis, P. Berg, A. Brand, and A. Wüest (2010), Application of oxygen eddy correlation in aquatic systems, *J. Atmos. Oceanic Technol.*, *27*, 1533–1546, doi:10.1175/2010JTECHO723.1.

Martin, W. R., M. Bender, M. Leinen, and J. Orchard (1991), Benthic organic carbon degradation and biogenic silica dissolution in the central equatorial Pacific, *Deep Sea Res. Part A*, *38*, 1481–1516, doi:10.1016/0198-0149(91)90086-U.

McGinnis, D. F., P. Berg, A. Brand, C. Lorrai, T. J. Edmonds, and A. Wüest (2008), Measurements of eddy correlation oxygen fluxes in shallow freshwaters: Towards routine applications and analysis, *Geophys. Res. Lett.*, *35*, L04403, doi:10.1029/2007GL032747.

McGinnis, D. F., S. Cherednichenko, S. Sommer, P. Berg, L. Rovelli, R. Schwarz, R. N. Glud, and P. Linke (2011), Simple, robust eddy correlation amplifier for aquatic dissolved oxygen and hydrogen sulfide flux measurements, *Limnol. Oceanogr. Methods*, *9*, 340–347, doi:10.4319/lom.2011.9.340.

Perlin, A., J. N. Moum, and J. Klymak (2005), Response of the bottom boundary layer over a sloping shelf to variations in alongshore wind, *J. Geophys. Res.*, *110*, C10S09, doi:10.1029/2004JC002500.

Pond, S. (1968), Some effects of buoy motion on measurements of wind speed and stress, *J. Geophys. Res.*, *73*(2), 507–512, doi:10.1029/JB073i002p00507.

Precht, E., U. Franke, L. Polarecky, and M. Huettel (2004), Oxygen dynamics in permeable sediments with wave-driven pore water exchange, *Limnol. Oceanogr.*, *49*, 693–705, doi:10.4319/lo.2004.49.3.0693.

Reimers, C. E., and R. N. Glud (2000), In situ chemical sensor measurements at the sediment-water interface, in *Chemical Sensors in Oceanography*, edited by M. S. Varney, pp. 249–282, Gordon and Breach, Amsterdam.

Reimers, C. E., R. A. Jahnke, and L. Thomsen (2001), *In situ* sampling in the benthic boundary layer, in *The Benthic Boundary Layer: Transport Processes and Biogeochemistry*, edited by B. P. Boudreau and B. B. Jørgensen, pp. 245–268, Oxford Univ. Press, New York.

Reimers, C. E., H. A. Stecher III, G. L. Taghon, C. M. Fuller, M. Huettel, A. Rusch, N. Ryckelynck, and C. Wild (2004), In situ measurements of advective solute transport in permeable shelf sands, *Cont. Shelf Res.*, *24*, 183–201, doi:10.1016/j.csr.2003.10.005.

Riedl, R. J., N. Huang, and R. Machan (1972), The subtidal pump: a mechanism of interstitial water exchange by wave action, *Mar. Biol. Berlin*, *13*, 210–221, doi:10.1007/BF00391379.

Rocha, C., S. Forster, E. Koning, and E. Epping (2005), High-resolution permeability determination and two-dimensional porewater flow in sandy sediment, *Limnol. Oceanogr. Methods*, *3*, 10–23, doi:10.4319/lom.2005.3.10.

Sakai, R. K., D. R. Fitzjarrald, and K. E. Moore (2001), Importance of low-frequency contributions to eddy fluxes observed over rough surfaces, *J. Appl. Meteorol.*, *40*, 2178–2192, doi:10.1175/1520-0450(2001)040<2178:IOLFCT>2.0.CO;2.

Schulz, H. D. (2006), Quantification of early diagenesis: Dissolved constituents in marine pore water and signals in the solid phase, in *Marine Geochemistry*, 2nd ed., edited by H. D. Schulz and M. Zabel, pp. 73–124, Springer, Berlin, doi:10.1007/3-540-32144-6_3.

Shaw, W. J., and J. H. Trowbridge (2001), The direct evaluation of near-bottom turbulent fluxes in the presence of energetic wave motions, *J. Atmos. Oceanic Technol.*, *18*, 1540–1557, doi:10.1175/1520-0426(2001)018<1540:TDEONB>2.0.CO;2.

Shum, K. T., and B. Sundby (1996), Organic matter processing in continental shelf sediments—The subtidal pump revisited, *Mar. Chem.*, *53*, 81–87, doi:10.1016/0304-4203(96)00014-X.

Strickland, J. D. H., and T. R. Parsons (1972), *A Practical Handbook of Seawater Analysis*, 2nd ed., Fish. Res. Board of Can., Ottawa, Canada.

Tengberg, A. (1997), Free-vehicle benthic lander technology for the study of biogeochemical processes in marine sediments, PhD thesis, Chalmers Univ. of Technol., Göteborg, Sweden.

Ullman, W. J., and R. C. Aller (1982), Diffusion coefficients in nearshore marine sediments, *Limnol. Oceanogr.*, *27*, 552–556, doi:10.4319/lo.1982.27.3.0552.

Verardo, D. J., P. N. Froelich, and A. McIntyre (1990), Determination of organic carbon and nitrogen in marine sediments using the Carlo Erba NA-1500 analyzer, *Deep Sea Res. Part A*, *37*, 157–165, doi:10.1016/0198-0149(90)90034-S.

Viollier, E., et al. (2003), Benthic biogeochemistry: State of the art technologies and guidelines for the future of in situ survey, *J. Exp. Mar. Biol. Ecol.*, *285–286*, 5–31, doi:10.1016/S0022-0981(02)00517-8.

Wheatcroft, R. A., and C. K. Sommerfield (2005), River sediment flux and shelf sediment accumulation rates on the Pacific Northwest margin, *Cont. Shelf Res.*, *25*, 311–332, doi:10.1016/j.csr.2004.10.001.

P. Berg, Department of Environmental Sciences, University of Virginia, PO Box 400123, Clark Hall, Balcony, Charlottesville, VA 22904, USA.

A. Devol, School of Oceanography, University of Washington, PO Box 355351, Seattle, WA 98195-7940, USA.

K. McCann-Grosvenor, H. T. Özkan-Haller, C. E. Reimers, and R. D. Sanders, College of Oceanic and Atmospheric Sciences, Oregon State University, 104 COAS Administration Bldg., Corvallis, OR 97331, USA. (creimers@coas.oregonstate.edu)